

Galaxy quenching timescales from a forensic reconstruction of their colour evolution

Matías Bravo^{1,2*}, Aaron S. G. Robotham^{1,3}, Claudia del P. Lagos^{1,3},
Luke J. M. Davies¹, Sabine Bellstedt¹ and Jessica E. Thorne¹

¹International Centre for Radio Astronomy Research (ICRAR), M468, University of Western Australia, 35 Stirling Hwy, Crawley, WA 6009, Australia.

²Department of Physics & Astronomy, McMaster University, 1280 Main Street W, Hamilton, ON, L8S 4M1, Canada

³ARC Centre of Excellence for All Sky Astrophysics in 3 Dimensions (ASTRO 3D).

Accepted XXX. Received YYY; in original form ZZZ

ABSTRACT

The timescales on which galaxies move out of the blue cloud to the red sequence (τ_Q) provide insight into the mechanisms driving quenching. Here, we build upon previous work, where we showcased a method to reconstruct the colour evolution of observed low-redshift galaxies from the Galaxy And Mass Assembly (GAMA) survey based on spectral energy distribution (SED) fitting with PROSPECT, together with a statistically-driven definition for the blue and red populations. We also use the predicted colour evolution from the SHARK semi-analytic model, combined with SED fits of our simulated galaxy sample, to study the accuracy of the measured τ_Q and gain physical insight into the colour evolution of galaxies. In this work, we measure τ_Q in a consistent approach for both observations and simulations. After accounting for selection bias, we find evidence for an increase in τ_Q in GAMA as a function of cosmic time (from $\tau_Q \sim 1$ Gyr to $\tau_Q \sim 2$ Gyr in the lapse of ~ 4 Gyr), but not in SHARK ($\tau_Q \lesssim 1$ Gyr). Our observations and simulations disagree on the effect of stellar mass, with GAMA showing massive galaxies transitioning faster, but is the opposite in SHARK. We find that environment only impacts galaxies below $\sim 10^{10} M_\odot$ in GAMA, with satellites having shorter τ_Q than centrals by ~ 0.4 Gyr, with SHARK only in qualitative agreement. Finally, we compare to previous literature, finding consistency with timescales in the order of couple Gyr, but with several differences that we discuss.

Key words: galaxies: evolution – software: simulations – techniques: photometric

1 INTRODUCTION

One of the most striking features of galaxies in the local Universe is the optical colour bimodality (e.g., Strateva et al. 2001; Blanton et al. 2003; Baldry et al. 2004; Driver et al. 2006), with most galaxies being either blue or red. Compared to these populations, there are comparatively few galaxies in the intermediate region, often referred to as the "green valley", (e.g., Martin et al. 2007; Wyder et al. 2007; Schawinski et al. 2014). Stars are the dominant source of the light emitted by most galaxies (at low redshift), suggesting that this bimodality is a consequence of the presence of two dominant stellar populations for galaxies. As the (intrinsic) colour of stars is mainly driven by their age, the colour bimodality is a reflection of a bimodality in the recent star formation in galaxies.

These populations are also characterised by intrinsically different galaxy properties. Red galaxies are preferentially of early-type morphology (e.g., Bershady et al. 2000; Mignoli et al. 2009; Schawinski et al. 2014), more massive (e.g., Baldry et al. 2004; Peng et al. 2010; Taylor et al. 2015), and found in denser environments (e.g., Kauffmann et al. 2004; Baldry et al. 2006; Peng et al. 2010). Studies have also shown that this bimodality is seen across cosmic time, with the fraction of galaxies in the red population increasing towards recent times (e.g., Wolf et al. 2003; Bell et al. 2004; Williams et al. 2009). It has also been found that the first galaxies that joined the red population are more massive than those that have joined at more recent times, a process called downsizing (e.g., Cowie et al. 1996; Brinchmann & Ellis 2000; Heavens et al. 2004). Combined, these observations present a broad picture where galaxies grow as part of the star-forming blue population, with some of them eventually ceasing to form stars and joining the red population (commonly

* E-mail: bravosam@mcmaster.ca

referred to as quenching, e.g., [Bell et al. 2004](#); [Blanton 2006](#); [Faber et al. 2007](#)).

The relative lack of galaxies located in the green valley implies short timescales to transition in colour (quench) for the galaxies that join the red population (e.g., [Schawinski et al. 2014](#); [Bremer et al. 2018](#)). Different mechanisms to quench star formation are expected to do so on different timescales (e.g., [Kaviraj et al. 2011](#); [Wetzel et al. 2013](#); [Schawinski et al. 2014](#); [Wheeler et al. 2014](#)), hence, studying these timescales can offer a view into the physical processes that govern galaxy evolution. Theoretical models are a critical tool to explore these mechanism, as we gain insight by testing their predictions against results from observations. A well-known example in the literature is that a quenching mechanism capable of stopping gas accretion onto galaxies is required to produce massive red galaxies, usually assumed to be driven by active galactic nuclei or shock heating of the halo gas (e.g., [Bower et al. 2006](#); [Cattaneo et al. 2006](#); [Croton et al. 2006](#); [Lagos et al. 2008](#)).

A historical challenge for simulations has been their inability to produce colour distributions well-matched to observations (e.g., [Weinmann et al. 2006](#); [Font et al. 2008](#); [Coil et al. 2008](#)), though recent advances have largely ameliorated this tensions (e.g., [Trayford et al. 2015](#); [Nelson et al. 2018](#); [Lagos et al. 2019](#); [Bravo et al. 2020](#)). These advances now enable the exploration of the colour evolution of galaxies with theoretical models, leading to the prediction of the timescales on which galaxies transition from being blue to red (e.g., [Trayford et al. 2016](#); [Nelson et al. 2018](#); [Wright et al. 2019](#)). This colour evolution is not directly measurable from observations and can only be inferred (e.g., [Schawinski et al. 2014](#); [Smethurst et al. 2015](#); [Rowlands et al. 2018](#); [Phillipps et al. 2019](#)). This means that results cannot be directly compared to the predictions of theoretical models. Further complicating comparisons is the lack of a unified definition for how to measure the colour transition timescales, or even what galaxies should be classified as blue or red (e.g., see classifications by [Martin et al. 2007](#); [Schawinski et al. 2014](#); [Taylor et al. 2015](#); [Bremer et al. 2018](#); [Wright et al. 2019](#)).

In [Bravo et al. \(2022, hereafter Paper I\)](#), we described a novel method to reconstruct the colour evolution of low-redshift observed galaxies from the Galaxy And Mass Assembly (GAMA; [Driver et al. 2011](#); [Liske et al. 2015](#)) survey, using the PROSPECT spectral energy distribution (SED) fitting tool ([Robotham et al. 2020](#)). We tested this recovery by performing the same procedure with a comparable sample of galaxies generated with the SHARK semi-analytic model (SAM; [Lagos et al. 2018, 2019](#)), finding that we can accurately recover the colour evolution of the last ~ 6 Gyr for galaxies with current masses above $\sim 10^9 M_{\odot}$. Finally, we provided a statistically-motivated definition for the blue and red populations, their evolution through cosmic time, and demonstrated the resulting probabilities of galaxies belonging to either blue or red population.

In this work we now utilise these results to explore how quickly galaxies transition from being blue to red, in a novel approach that is consistent and directly comparable for both observations and simulations. In Section 3 we explore the distribution of probabilities of galaxies being red, to construct statistically-motivated definitions for when a galaxy is certainly a member of either population, and when is transitioning between both. We then use that classification to explore the timescale on which galaxies transitioned from blue to red in Section 4, exploring possible time, mass, and environmental effects. For conciseness, we will refer to this blue-to-red transition timescale as τ_Q throughout this work. In Section 5 we discuss our results, both for the physical implications of the timescales we measure and to compare with the existing literature. Finally, we present our conclusions in Section 6. In this work, we adopt the

[Planck Collaboration et al. \(2016\)](#) Λ CDM cosmology, with values of matter, baryon, and dark energy densities of $\Omega_b = 0.0488$, and $\Omega_{\Lambda} = 0.6879$, respectively, and a Hubble parameter of $H_0 = 67.51 \text{ km s}^{-1} \text{ Mpc}^{-1}$.

2 GALAXY CATALOGUES

In this work, we use the data set presented in [Paper I](#), which we briefly outline. This data set is composed of the intrinsic colour (i.e., not attenuated by dust) and stellar mass histories for three low-redshift galaxy samples, both derived from their star formation and metallicity histories (SFH and ZH, respectively). The first one is comprised of $\sim 7,000$ galaxies from the GAMA survey used in [Bellstedt et al. \(2020, 2021\)](#). The other two are each comprised of $\sim 30,000$ GAMA-like galaxies (i.e., $r_{\text{apparent}} < 19.8 \text{ mag}$) from the SHARK SAM ([Lagos et al. 2018, 2019](#)). For the GAMA sample, we reconstructed their colour evolution from the star formation and metallicity histories inferred from the SED fitting by [Bellstedt et al. \(2020\)](#)¹ by combining these histories with the stellar population synthesis model used for the fitting ([Bruzual & Charlot 2003](#)). The two SHARK samples contain the same galaxies, the difference is how we constructed the colour and stellar mass evolution: one sample is the predicted evolution from the simulation itself (which we will refer as SHARK); the other presents the inferred evolution from SED fitting the SHARK galaxies with the same method as with the GAMA sample (we will refer to this sample as SHARK_{fit}). Section 2 of [Paper I](#) contains the detailed description of these three samples, with Appendix A offering a deeper exploration of our SED modelling choices for the interested reader.

Inspired by [Taylor et al. \(2015\)](#), in [Paper I](#) we modelled the colour-mass distribution for each sample with a time-and-mass-dependent Gaussian Mixture Model (GMM). Consistent with the modelling by [Baldry et al. \(2004\)](#) and [Taylor et al. \(2015\)](#), we described the colour-mass distribution of galaxies in [Paper I](#) with two evolving populations: blue and red². These GMMs are described by five parameters: the relative fraction of blue (or red) galaxies, and the means and standard deviations of each population. In [Paper I](#) we presented a two-step parameterisation of these parameters, first as a function of stellar mass, and second as a function of lookback time. For the stellar mass parameterisation, based on the distributions of the GMM parameters as a function of stellar mass, we chose to parameterise the relative blue/red fractions with a logistic curve, and with first-order polynomials for the means and standard deviations. We then parameterised the time evolution of the stellar mass-dependent Gaussian parameters, using second- and third-order polynomials. Section 3 of [Paper I](#) provides the complete description of this modelling, with section 3.1, figure 2 and table 1 offering an simple overview.

With a complete parameterisation of the evolution of the colour

¹ The SFH model adopted by [Bellstedt et al. \(2020\)](#) is a skewed Gaussian, a parametric model but significantly more flexible than other common parametric models in the literature (e.g., [da Cunha et al. 2008](#); [Noll et al. 2009](#); [Carnall et al. 2018](#); [Boquien et al. 2019](#)), but still unable to model rejuvenation episodes. While not unique among SED fitting models (e.g., [Carnall et al. 2018](#); [Johnson et al. 2021](#)), the use of PROSPECT in the literature has been unique in the assumption that gas metallicities *evolves*, modelling it as a linear scaling of the mass growth of galaxies ([Bellstedt et al. 2020](#); [Thorne et al. 2021, 2022](#)).

² We did test using three components, but we found no statistical evidence for a third (green) population. See section 3.3 of [Paper I](#) for further details.

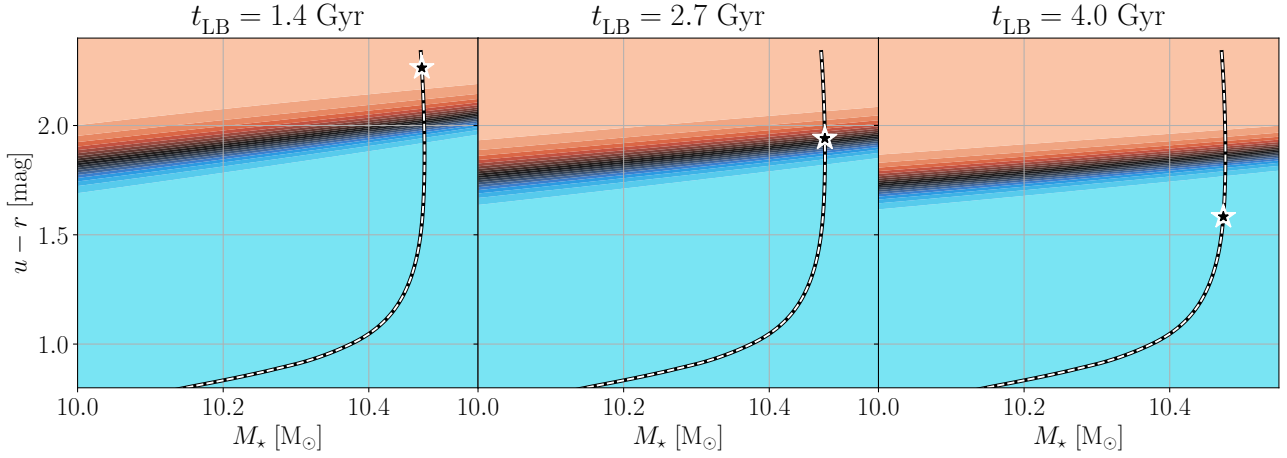


Figure 1. The colour evolution of a single galaxy and its transition from the blue to the red population from the results Paper I, with the galaxy CATAID=92739 from the GAMA survey used for this example. Each panels shows a small section of the colour-mass plane for the GAMA survey at three different lookback times, with the coloured contours showing the probability of being red for a galaxy in any given position in this space. The complete evolution track of the galaxy is shown by the black and white line running from the bottom left to the top right of each panel, with the position of the galaxy in the corresponding lookback time of each panel shown with a star marker.

populations for all three samples, we can calculate the probability for any galaxy belonging to the blue or red population at any given time. As in figure 12 of Paper I, in this work we choose to show the probability of being red, P_R^3 , which is calculated from the Gaussian Mixture Model with which we model the galaxy colour distribution (see sections 3.3 and 3.4 of Paper I for further details).

We also showed that our colour-based classification leads to a sensible separation in specific star formation rate as a function of stellar mass. The transition zone is not cleanly defined in this space, as expected from the scatter between colour and specific star formation rate. In Paper I, through the comparison of the colour evolution of the three samples (GAMA, SHARK, and SHARK_{fit}), we found that the reconstruction of the colour evolution becomes biased by the modelling choices in the SED fitting for lookback times above ≥ 6 Gyr. For this reason, while we will measure colour evolution from a lookback time of 10 Gyr onward and show some of our results at higher lookback times, we mainly focus on the τ_Q we measure below a lookback time of 6 Gyr.

In this work, we use P_R to calculate τ_Q , defining the lookback times when a galaxy leaves the blue population ($t_{LB,B}$) and when it joins the red population ($t_{LB,R}$), which are related to τ_Q as:

$$\tau_Q = t_{LB,B} - t_{LB,R}, \quad (1)$$

where we define these lookback times such that $t_{LB,B} > t_{LB,R}$ (i.e., $\tau_Q > 0$). In Paper I we chose a time step of 100 Myr to reconstruct the colour evolution of galaxies, meaning that the shortest measurable τ_Q is 100 Myr. Figure 1 shows an example of the data set we constructed in Paper I and use in this work to measure τ_Q , with both the evolutionary tracks in the colour-mass plane of individual galaxies and our model to calculate P_R at any point in the $t_{LB}-M_*$ - $(u-r)$ space. Our example galaxy moves from being likely blue

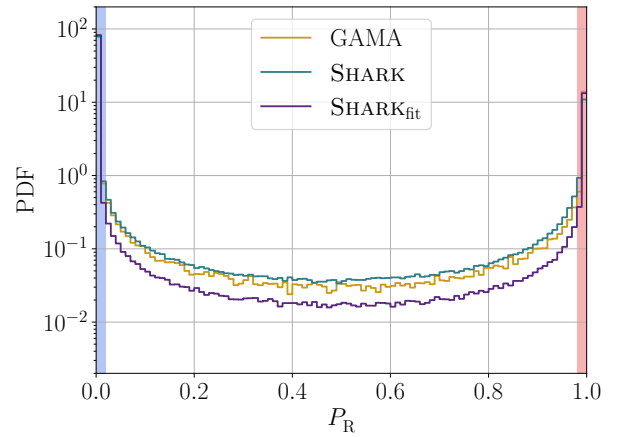


Figure 2. Distribution of probability of being red for all galaxies and all time steps below 6 Gyr. As in Paper I, the orange line shows the distribution for GAMA, cyan for SHARK, and purple for SHARK_{fit}. Each bin spans 1% in probability. Highlighted in blue/red are the probability ranges where we define a galaxy as being blue/red ($P_R = 0.02$ and $P_R = 0.98$, respectively).

until a lookback time of ~ 4 , to have a similar probability of being either blue or red at ~ 2.7 Gyr ($P_R \sim 0.5$), to likely becoming red at ~ 1.5 Gyr. What is not immediately obvious from this Figure alone is what values of P_R best define $t_{LB,B}$ and $t_{LB,R}$, which is the first aspect we will address in Section 3.

3 DISTRIBUTION AND EVOLUTION OF THE PROBABILITY OF GALAXIES BEING RED

With the probabilistic blue/red classification from Paper I, the last step needed to measure τ_Q is the choice of probabilities at which a

³ Formally the probability of being red is a function of lookback time, stellar mass, and colour, but for brevity we will refer to it as P_R instead of $P_R(t_{LB}, M_*, u-r)$.

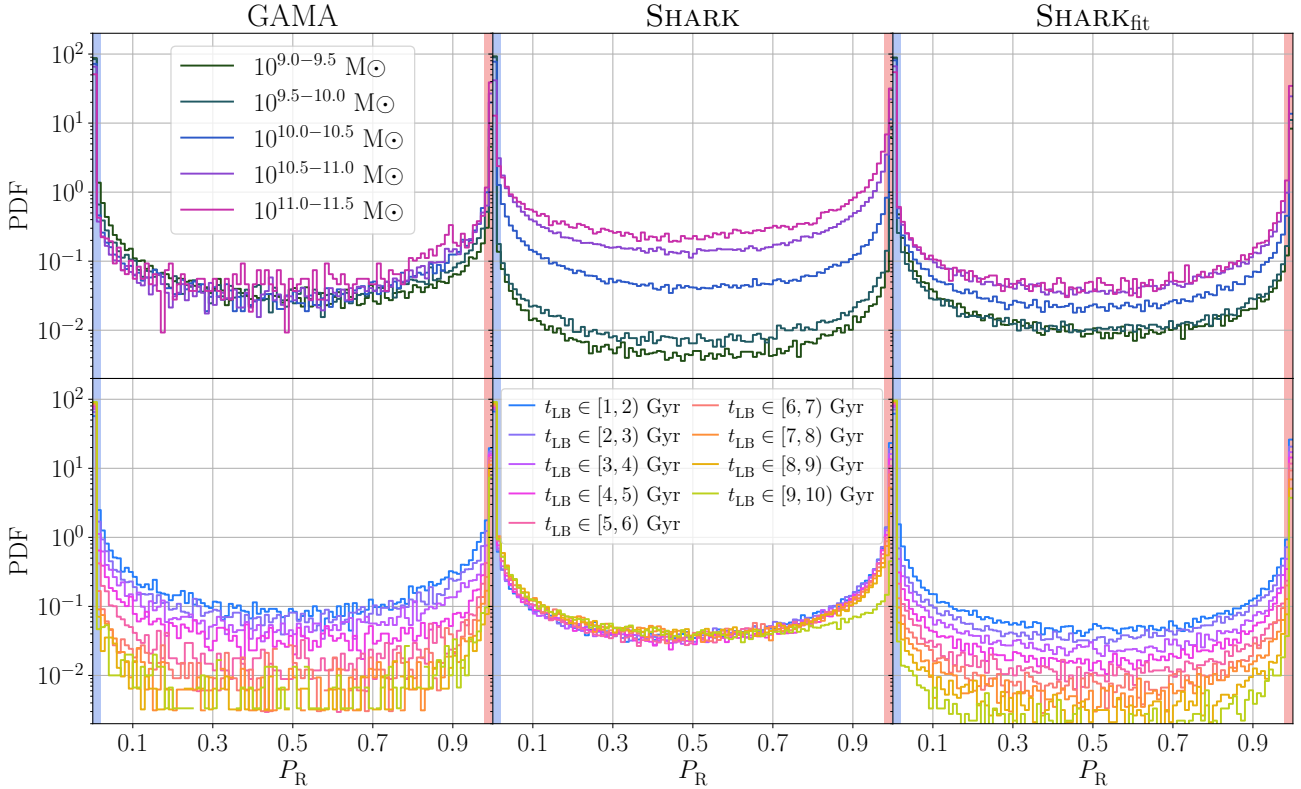


Figure 3. Distribution of the probability of galaxies being red. Each column shows the probability distribution for single sample, from left to right: GAMA, SHARK, and SHARK_{fit}. The top row shows the distribution at all time steps below 6 Gyr binned by stellar mass at observation time, with bins of increasing mass shown with lighter colours. The bottom row shows the distribution at all stellar masses binned by lookback time, with bins of increasing lookback time in lighter colours. Highlighted in blue (red) are the probability ranges where we define a galaxy as being blue (red), as in Figure 2.

galaxy is considered to be a part of the blue or red populations. While ultimately this is an arbitrary choice, we will use the distribution of our calculated probabilities to inform this choice, just like our choice of a GMM to describe the colour populations in Paper I was informed by the reconstructed colour distributions. As the green valley is sparsely populated, most of the mass of the PDF will be near the edges (i.e., near $P_R = 0$ and $P_R = 1$). We use the second derivative of the decrease of the PDF from the edges towards the centre as a guide for our choice. Figure 2 shows the distribution of probabilities of being red (P_R), stacked from all time steps and stellar masses given our selection criteria. The transition from the extremes of the probability range is dramatic, with a ~ 2 dex (~ 1 dex) decrease in the PDF from the 0-1% bin (99-100%) to the 1-2% bin (98-99%). This would suggest $P_R < 0.01$ ($P_R > 0.99$) is a reasonable criterion for a galaxy to be confidently classified as blue (red).

While such a selection will work on average, the distribution of probabilities may depend on stellar mass and/or lookback time. To examine this, Figure 3 shows the probability distributions for all samples binned by both stellar mass and lookback time. GAMA and SHARK show opposite trends, with the former exhibiting a probability distribution that is mass-independent but time-dependent, and the latter being mass-dependent but time-independent. This difference suggests that we expect a stellar mass trend for τ_Q in SHARK, and a lookback time trend in GAMA. SHARK_{fit} exhibits a mix of the trends in GAMA and SHARK, suggesting that our modelling choices

in PROSPECT may be impacting our τ_Q measurements, but also that they are not completely dictated by them.

While for most of the PDFs shown, a choice of $P_R < 0.01$ ($P_R > 0.99$) would still lead to a strong blue (red) classification, this is not true for the two highest mass bins in SHARK. For this reason we will use a more conservative classification of $P_R < 0.02$ for blue galaxies, $P_R > 0.98$ for red galaxies, for the rest of this work (see also the bottom row of Table 3). We note that small variations to these limits do not affect the qualitative nature of our results, nor do they lead to strong quantitative changes.

3.1 Time evolution of the fractions of blue, transitional, and red galaxies

We explore the fractions of galaxies in blue/transitional/red regions across cosmic time in Figure 4. We also show in Figure 4 the fractions for both central and satellite galaxies, according to their classification at observation time. For this, we follow the same convention adopted in Bravo et al. (2020) of treating all isolated and central group galaxies⁴ from GAMA as centrals, and the remaining galaxies as satellites. Since we demonstrated in that work that central/satellite

⁴ Those with RankIterCen = 1 in the GAMA Galaxy Group Catalogue, from the iterative ranking procedure defined in section 4.2.1 of Robotham et al. (2011).

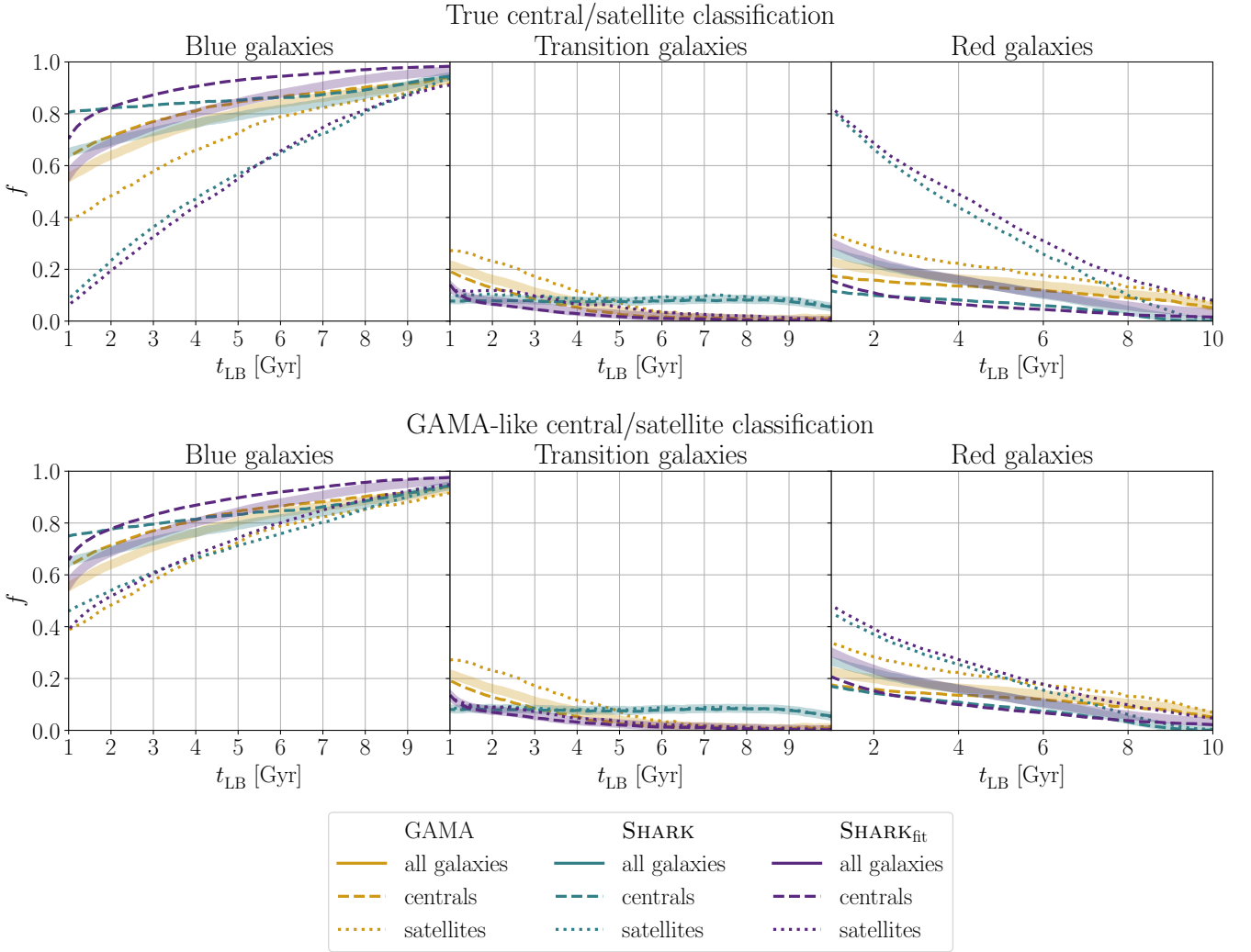


Figure 4. Time evolution of the fraction of galaxies classified as blue/transitional/red, as a function of the central/satellite classification for SHARK and SHARK_{fit}. Galaxies included correspond to those above the evolving mass completeness limits at $z \sim 0.06$ defined in Paper I (see their section 3.2), corresponding to $M_{\star}(z \sim 0.06) \geq 10^{9.1} M_{\odot}$ for GAMA and $M_{\star}(z \sim 0.06) \geq 10^{9.0} M_{\odot}$ for SHARK/SHARK_{fit}. Each column shows a different population: blue in the left column, transitional in the middle, and red in the right. In each panel the corresponding population is shown for our three samples, with the combined central+satellite fraction is shown in solid lines, centrals only with dashed lines, and satellites with dotted lines. SHARK and SHARK_{fit} are shown in the top row using the central/satellite classification from the simulation, and using a GAMA-like classification in the bottom row (23% confusion, following the results from Bravo et al. 2020; Chauhan et al. 2021). Line colours are as in Figure 2. Columns are as in Figure 3. The results for GAMA are identical in each column, they are repeated for easier comparison with both classifications from the simulations.

Selected galaxies	GAMA	SHARK	SHARK _{fit}
Are red by $t_{\text{LB}} = 1$ Gyr	22.9%	26.7%	30.2%
Became red at $t_{\text{LB}} < 10$ Gyr	15.0%	< 26.0%	21.2%
Were blue at $t_{\text{LB}} = 10$ Gyr and are red at $t_{\text{LB}} = 1$ Gyr	14.3%	22.2%	21.0%

Table 1. Percentage of the total population of galaxies that are currently red, that became red after $t_{\text{LB}} = 10$ Gyr, and that transitioned from blue to red after $t_{\text{LB}} = 10$ Gyr, from all three samples. The bottom row is the sample selected to measure τ_{Q} .

confusion plays is an important factor, we show the results for both the true central/satellite classification in SHARK/SHARK_{fit} and a confused classification. We note that we use a higher level of confusion than in Bravo et al. (2020), 23% instead of 15%, because the sample we use from GAMA in this work is limited to a significantly lower redshift ($z < 0.06$ instead of $z < 0.6$). This elevated confusion can

be seen in figure 3 of Bravo et al. (2020), and we first presented and tested this higher value in Chauhan et al. (2021).

The time dependence (independence) of the density for intermediate values of P_{R} seen for GAMA and SHARK_{fit} (SHARK) in Figure 3 is clearly reflected in the time evolution of the transitional fraction of galaxies shown in Figure 4. The red fraction is in excel-

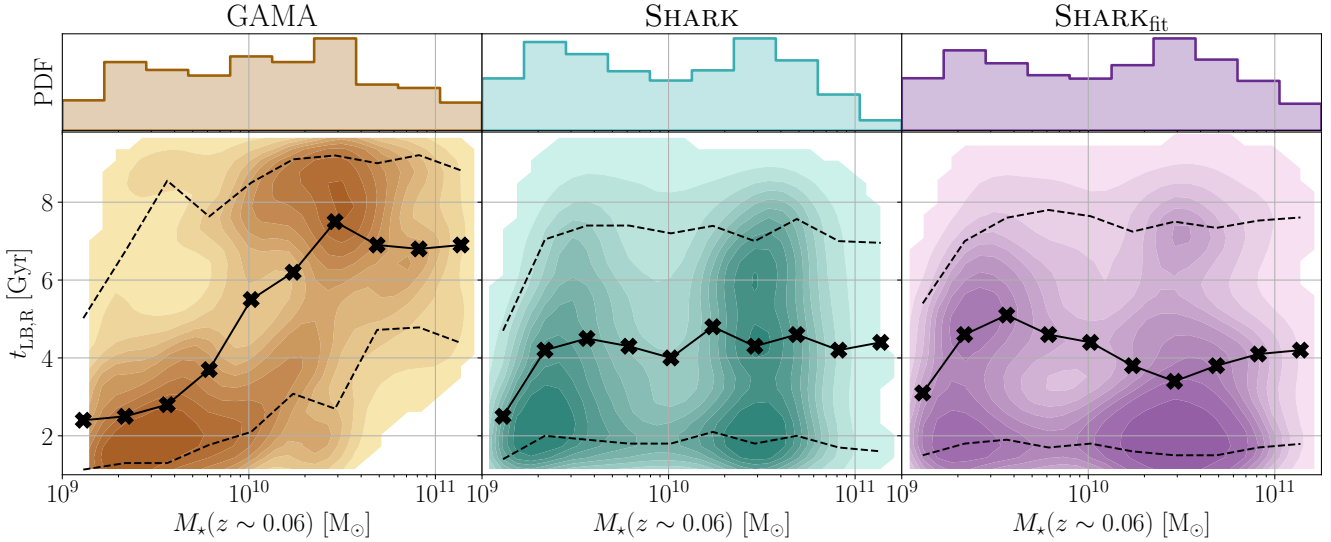


Figure 5. The lookback time when (currently red, $z \sim 0.06$) galaxies joined the red population ($t_{\text{LB,R}}$) as a function of current stellar mass, together with the stellar mass distribution, for each of our samples selected following Table 1. For each individual sample, the solid lines indicates the $t_{\text{LB,R}}$ running median, the dashed lines the running 16-84th percentiles, both using the same bins as the stellar mass histograms of the top panels. The black markers indicate the stellar mass and $t_{\text{LB,R}}$ median point for each bin. The background contours indicate the smooth distribution obtained using the `gaussian_kde` Gaussian Kernel Density Estimator (KDE) function from `scipy`, to avoid visualisation artefacts due to the discreteness of our data in $t_{\text{LB,R}}-\tau_{\text{Q}}$ space. The lightest contour shows the highest-density region containing 99% of the mass of the Gaussian KDE, with the rest of the contours evenly spaced in percentage of the mass contained.

lent agreement between *SHARK* and *SHARK_{fit}*, which indicates that we are accurately recovering this fraction with *PROSPECT*. In contrast, the transitional fractions in *SHARK_{fit}* are in better agreement with *GAMA* than *SHARK*, suggesting that this is to some degree affected by the modelling choices in *PROSPECT*. We note that the increased blue fraction in *SHARK_{fit}* is consistent with the delayed SFHs relative to those of *SHARK* that we showed in appendix A of Paper I, an issue we found related to a hard-to-solve degeneracy between dust and star formation parameters for bulge-dominated massive galaxies in *SHARK*.

Central galaxies show a higher blue fraction than satellites in all samples, but there are differences across samples. *SHARK* and *SHARK_{fit}* predict a higher fraction of blue centrals relative to *GAMA*, at lookback times of $\lesssim 5$ Gyr for the former and at all lookback times for the latter, though including central/satellite classification confusion lessens this tension. The opposite trend is true for the red population, being under-estimated by *SHARK*/*SHARK_{fit}* compared to *GAMA*. Interestingly, while *SHARK_{fit}* shows a strong under-prediction of the transitional fraction of centrals at ≥ 3 Gyr relative to *SHARK*, the difference is mostly absorbed by the blue fraction, which is overestimated (underestimated) in *SHARK_{fit}* above (below) a lookback time of ~ 2 Gyr. This points to the $t_{\text{LB,B}}$ recovered for centrals being biased towards later times.

SHARK and *SHARK_{fit}* exhibit a significantly higher fraction of red satellites compared to *GAMA*, reaching $\sim 80\%$ at $t_{\text{LB}} = 1$ Gyr, a factor of ~ 3 larger than observations, but this tension is strongly reduced when accounting for central/satellite classification confusion. The transitional satellites in *SHARK_{fit}* show a similar difference to those in *SHARK* as previously mentioned for centrals, but unlike centrals, the under-abundance of transitional satellites in *SHARK_{fit}* is balanced out by an over-abundance of both blue and red satellites. This difference suggests that the SFH model parameterisation adopted in *PROSPECT* may cause the transition measured to be too fast. *GAMA* and *SHARK_{fit}* exhibit a qualitatively

similar evolution for the transition fraction, and they come into quantitative agreement at lookback times of ≥ 6 Gyr, in line with the results from Paper I.

4 DISTRIBUTION AND TIME EVOLUTION OF τ_{Q}

Defining both $t_{\text{LB,B}}$ and $t_{\text{LB,R}}$ is straightforward for *GAMA* and *SHARK_{fit}*, as P_{R} is monotonically-increasing due to our choice of SFH in *PROSPECT*, with $t_{\text{LB,B}}$ ($t_{\text{LB,R}}$) simply being the last (first) time the galaxy was a member of the blue (red) population. The caveat to this statement is that, depending on the details of the evolution of the galaxy colour populations as a whole, a galaxy may see a decrease in P_{R} without changing its colour. We do observe this behaviour in both *GAMA* and *SHARK_{fit}*, being particularly clear for galaxies above $\sim 10^{10.5} M_{\odot}$ in the former. For this reason, we force a monotonic time evolution of P_{R} for galaxies that cross our $P_{\text{R}} = 0.98$ threshold in these two samples. We find the maximum P_{R} for all galaxies after they become red, and then set all subsequent values of P_{R} to this maximum value.

SHARK SFHs are not forced to be monotonic, and while rejuvenation in *SHARK* is not a common occurrence in general ($\lesssim 3\%$, see Appendix A2 of Paper I), the measurement of τ_{Q} for galaxies that do rejuvenate presents a challenge (mostly massive centrals). To measure τ_{Q} in *SHARK*, we first select galaxies that are blue at $t_{\text{LB}} = 10$ Gyr and that are red $t_{\text{LB}} = 1$ Gyr, trace the continuous time span during which the galaxy was red, and the latest time before this period that the galaxy was blue (see Appendix A for a discussion on different definitions). Table 1 shows the fraction of red galaxies in our three samples, indicating that selecting galaxies being blue at least at a lookback time of 10 Gyr discards $\sim 20\text{--}40\%$ of the current red galaxies, with *GAMA* seeing the largest reduction in sample size and *SHARK* the smallest.

Before we explore the measured τ_{Q} from our samples, we

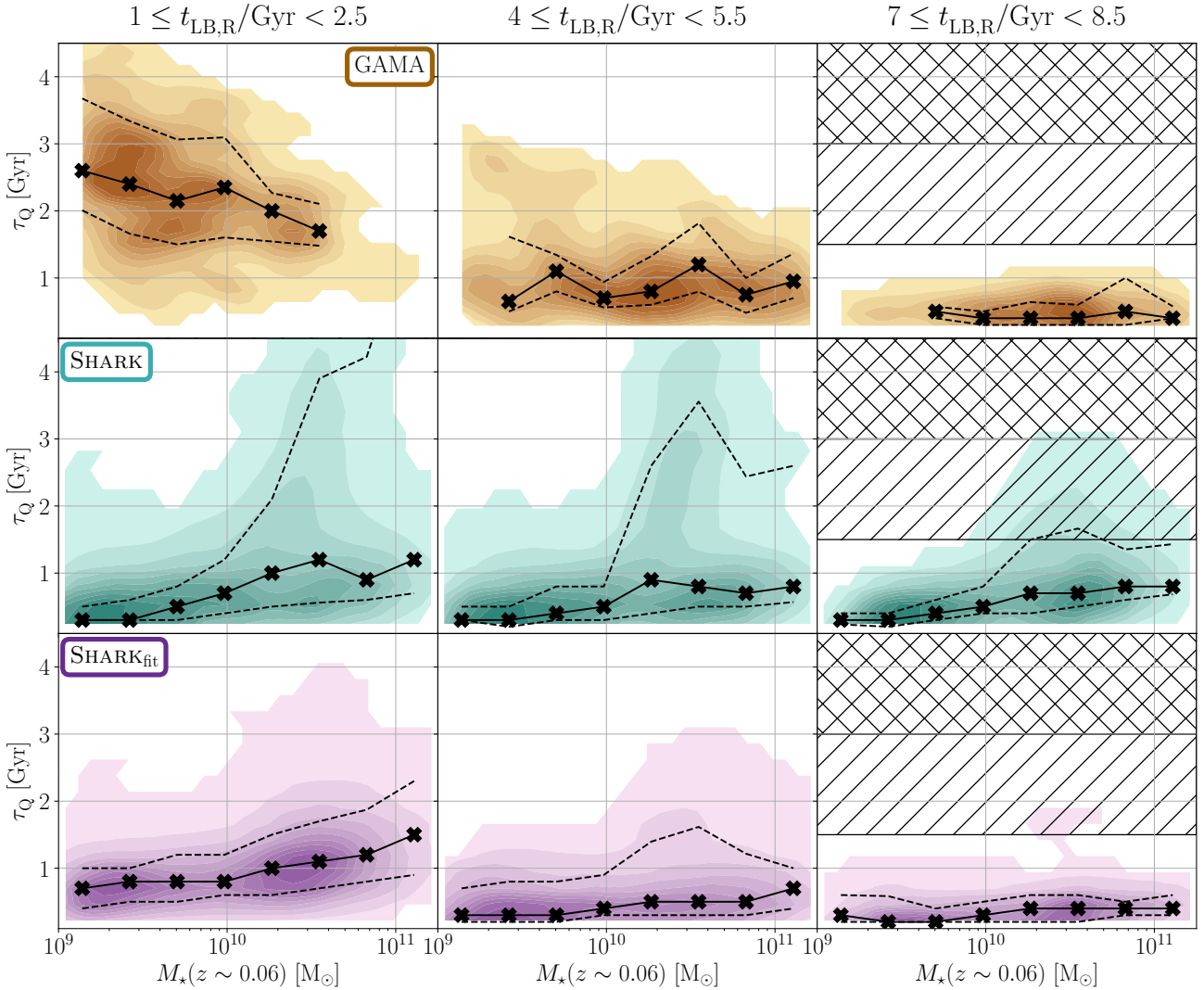


Figure 6. Blue-to-red transition timescales (τ_Q) as a function of current stellar mass. The distributions are shown for three $t_{LB,R}$ bins: $1 \leq t_{LB,R} < 2.5$ (left column), $4 \leq t_{LB,R} < 5.5$ (middle column), and $7 \leq t_{LB,R} < 8.5$ (right column). Each row corresponds to a different sample, from top to bottom: GAMA, SHARK, and SHARK_{fit}. Solid lines, dashed lines, markers and contours as in Figure 5. The diagonally-hatched region indicates where the τ_Q measurements become incomplete in the corresponding $t_{LB,R}$ bin, and the cross-hatched where no τ_Q measurement is possible (only visible on the right-most column due to our choice of limits for the y-axis). Note that the $t_{LB,R}$ bin shown in the left column lies in the range of lookback times that we found affected by SED-fitting-related biases in Paper I.

first discuss the $t_{LB,R}$ distributions in Figure 5. While all three samples display roughly similar stellar mass distributions for red galaxies (though SHARK/SHARK_{fit} show a bimodality not clear in GAMA), there are differences in when these galaxies became red. GAMA exhibits a clear trend in $t_{LB,R}$ with stellar mass, with more massive galaxies becoming red at earlier times. In contrast, the $t_{LB,R}$ distribution in both SHARK and SHARK_{fit} are broadly consistent for stellar masses above $\gtrsim 9.3$ Gyr, i.e., the time when SHARK galaxies become red shows no clear trend with stellar mass. The overall good agreement between both SHARK and SHARK_{fit} indicates that there are no strong biases in our GAMA measurements, hence the strong difference between GAMA and SHARK/SHARK_{fit} is not a consequence of our colour evolution reconstruction. In other words, the fact that we do not find a downsizing trend in SHARK/SHARK_{fit}

as strong as in GAMA is a short-coming of the physical models in SHARK⁵

⁵ The reader may find this tension to resemble the historical one of too many star-forming massive galaxies addressed in the works of, e.g., Bower et al. (2006); Cattaneo et al. (2006); Croton et al. (2006). These works proposed solutions to (then current) tension in the fraction of $z \sim 0$ massive passive galaxies, i.e., *how many* massive red galaxies the early galaxy formation models. The tension we find in this work is in the $t_{LB,R}$ distribution of $z \sim 0$ massive passive galaxies, i.e., *when* massive passive galaxies became red. Hence, our findings showcase the need for second-order corrections to the modelling of galaxy formation relative to those presented in Bower et al. (2006); Cattaneo et al. (2006); Croton et al. (2006).

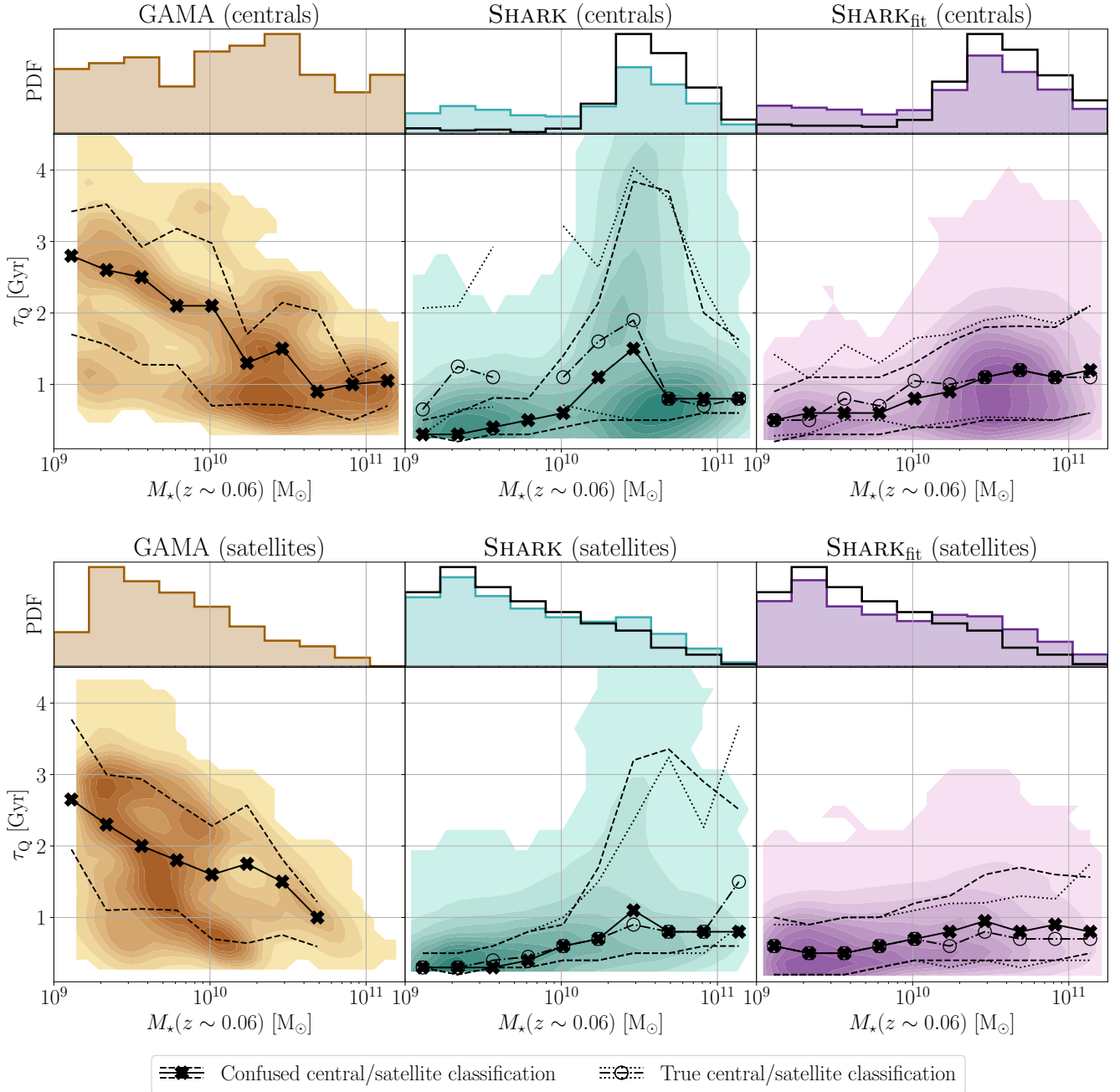


Figure 7. τ_Q as a function of current stellar mass, together with the stellar mass distribution, divided between centrals and satellites. Only galaxies with $1 \leq t_{\text{LB,R}} < 6$ Gyr are shown. For each individual sample, the solid/dashed (dash-dotted/dotted) lines indicate the τ_Q running median/16-84th percentiles for the GAMA-like (true) central-satellite classification, both using the same bins as the stellar mass histograms. The black cross (open) markers indicate the stellar mass and $t_{\text{LB,R}}$ median point for the GAMA-like (true) central-satellite classification in each bin. Contours as in Figure 5. The coloured (black) histograms show the measured stellar mass distribution for the GAMA-like (true) central-satellite classification. Note that the gap seen in the running median for the true centrals in SHARK corresponds to a mass bin where no galaxies are present (see histogram above).

4.1 τ_Q distribution of the overall galaxy population

In Figure 6 we show the distribution of τ_Q as a function of stellar mass, divided into three lookback time bins. The distributions are roughly consistent across cosmic time in SHARK, the largest difference being the increased dispersion above $\sim 10^{10} M_\odot$, which suggests that there is no strong time evolution of the τ_Q distribution.

In contrast, the τ_Q distribution of GAMA changes as a function of $t_{\text{LB,R}}$, with the median τ_Q increasing by a factor of ~ 3 in the span of 4.5 Gyr.

GAMA and SHARK_{fit} display similar timescale-mass relations in the highest $t_{\text{LB,R}}$ bin. This is in line with the results in Paper I, where we found a strong similarity in the galaxy distributions of both GAMA and SHARK_{fit} in colour-mass space at high lookback

times ($t_{\text{LB}} > 6$ Gyr), likely driven by dust parameter degeneracies (see Appendix A of Paper I for further details). The timescale-mass relations measured in SHARK and SHARK_{fit} are in good agreement in the other two lookback time bins, indicating that we can recover this with PROSPECT, which validates the difference between both and GAMA as real. The only significant difference between SHARK and SHARK_{fit} at these lower lookback times is that we do not recover the longest τ_{Q} from SHARK, possibly due to episodes of weak rejuvenation extending the time period galaxies remain in the transitional region. The $\tau_{\text{Q}}-M_{\star}$ relation that we observe in GAMA is in clear tension with that we predict in SHARK, which also exhibit opposite trends with stellar mass, i.e., low-mass galaxies in GAMA take much longer to quench at recent times than in SHARK. We explore the effect of selection biases in the measured τ_{Q} evolution in Appendix B, where we find that GAMA does exhibit a strong time evolution of the τ_{Q} distribution, a mild evolution in SHARK_{fit}, and that the τ_{Q} distribution in SHARK is independent of cosmic time.

4.2 Environmental effects on τ_{Q}

We now explore how τ_{Q} compares between central and satellite galaxies. Figure 7 shows both the stellar mass distribution and τ_{Q} as a function of their current stellar mass, divided into centrals and satellites. For SHARK and SHARK_{fit} we show the results for both true and GAMA-like central/satellite classifications.

True centrals and satellites in SHARK show a significant difference in τ_{Q} for galaxies below $\sim 10^{10.5} M_{\odot}$, with centrals exhibiting longer timescales than satellites. Satellites in SHARK_{fit} are in good agreement with those from SHARK. Centrals show less of an agreement for τ_{Q} , in particular the timescales in SHARK_{fit} for centrals of $\sim 10^{9.5} M_{\odot}$ ($\sim 10^{10.5} M_{\odot}$) are shorter than in SHARK by a factor of ~ 4 (~ 2). In comparison, GAMA centrals and satellites only differ at $M_{\star} \lesssim 10^{10} M_{\odot}$, with τ_{Q} of satellites being ~ 0.4 Gyr than for centrals. The difference between centrals and satellites is reduced when using a GAMA-like classification for both SHARK and SHARK_{fit}, suggesting the possibility of a larger difference between GAMA centrals and satellites than what we measure.

To further explore the differences for satellites between GAMA and SHARK, Figure 8 shows the mass distribution of haloes that host satellites in both samples. To quantify the differences between GAMA and SHARK, Table 2 contains the first Wasserstein distances between the several selections shown in Figure 8. Chauhan et al. (2021) found that the recovery of SHARK halo masses with the Robotham et al. (2011) group finder, which was used to infer halo masses for GAMA, is reasonable for the high-multiplicity groups ($N_g \geq 5$) but the quality of the recovery noticeably decreases for low-multiplicity groups. Those results can account for the difference between GAMA and SHARK in the distribution of halo masses for haloes hosting at least one satellite. The GAMA and SHARK halo mass distributions for all groups hosting at least one satellite are significantly different, irrespective of the P_{R} selection applied to both samples, with similar first Wasserstein distances. The relative distribution of blue/red galaxies are also different, with the majority of haloes in SHARK that host at least one satellite also hosting at least one red satellite, in strong contrast to GAMA.

Figure 8 and Table 2 show that the halo mass distribution of $N_g \geq 5$ groups with red satellites in GAMA and SHARK are significantly closer, hence this should be a strong probe for the treatment and evolution of the satellites residing in such haloes. For centrals, we ignore $N_g \geq 5$ group red centrals, as there are $\lesssim 40$ of

Selection	Wasserstein distance
All haloes	0.275
All haloes, blue satellites	0.306
All haloes, transitional satellites	0.231
All haloes, red satellites	0.267
$N_g \geq 5$ haloes, blue satellites	0.246
$N_g \geq 5$ haloes, transitional satellites	0.267
$N_g \geq 5$ haloes, red satellites	0.105

Table 2. The Wasserstein distance between the each corresponding pair for the GAMA and SHARK halo mass distributions shown in Figure 8.

the latter in GAMA and SHARK⁶. Overall, we find little difference between true central (all true satellite) and isolated ($N_g \geq 5$ satellite) galaxies in all three samples, with the most important finding being that SHARK/SHARK_{fit} lack the observed numbers of $\lesssim 10^{10} M_{\odot}$ red isolated galaxies we find in GAMA (see Figure included in the supplemental material).

4.3 Connection between τ_{Q} and satellite infall in SHARK

One of the powerful features of using simulations is that they enable us to further explore the evolution of red galaxies. In particular, here we explore how τ_{Q} is linked to the central-to-satellite transition in SHARK, with which we explore the effect of implemented physical models in driving τ_{Q} . While we can also explore this aspect with SHARK_{fit}, Appendix A shows that there are reasons not to. Both $t_{\text{LB,B}}$ and $t_{\text{LB,R}}$ are not as well-recovered as τ_{Q} , which leads to significant confusion on whether a satellite became red before, during, or after infall, e.g., the percentage of the former increases from $\sim 4\%$ to $\sim 15\%$. Classifying whether a SHARK_{fit} satellite became red based on $t_{\text{LB,R}}$ measured in SHARK would limit our analysis to how well we recover the evolution of centrals and satellites (see Appendix A). For GAMA, this effect would be further compounded by the relatively limited ability to extract infall times from observations⁷.

We classify satellite galaxies in SHARK in three groups, based on the lookback time of infall ($t_{\text{LB,infall}}$) relative to its transition from blue to red, those that:

- (i) became red before they became a satellite, i.e., transitioned in colour before infall, $t_{\text{LB,B}} > t_{\text{LB,R}} > t_{\text{LB,infall}}$;
- (ii) were a central the last time they were blue, but were a satellite by the time they became red, i.e., infall happened during the colour transition, $t_{\text{LB,B}} > t_{\text{LB,infall}} > t_{\text{LB,R}}$;

⁶ There are significantly more in SHARK_{fit}, factor of ~ 4 more than in SHARK, but this is a consequence of the delayed formation of the red population from our PROSPECT fits to SHARK. This could be a result of the relative fractions of galaxies that undergo rejuvenation, as defined in Paper I, as $\sim 20\%$ of the red centrals in SHARK had at least one rejuvenation episode, compared to only $\sim 4\%$ of satellites. We should also note that we are using a subset of the full simulation box for SHARK/SHARK_{fit}, so it is possible to increase this number by a factor of ~ 30 . The low number from GAMA is the limit to study $N_g \geq 5$ group red centrals.

⁷ E.g., the method outlined in Pasquali et al. (2019) divides phase-space into a series of distinct regions characterised by a monotonically-increasing mean time of infall. The main limitation of such methods is the significant overlap in infall times ranges between zones. Furthermore, we note to the reader that τ_{Q} , $\Delta t_{\text{LB,B}}$ and $\Delta t_{\text{LB,R}}$, and the scatter in the infall time found by Pasquali et al. (2019) are all in the order of ~ 2 Gyr, which we expect to strongly obscure the correlation between infall and quenching, if present.

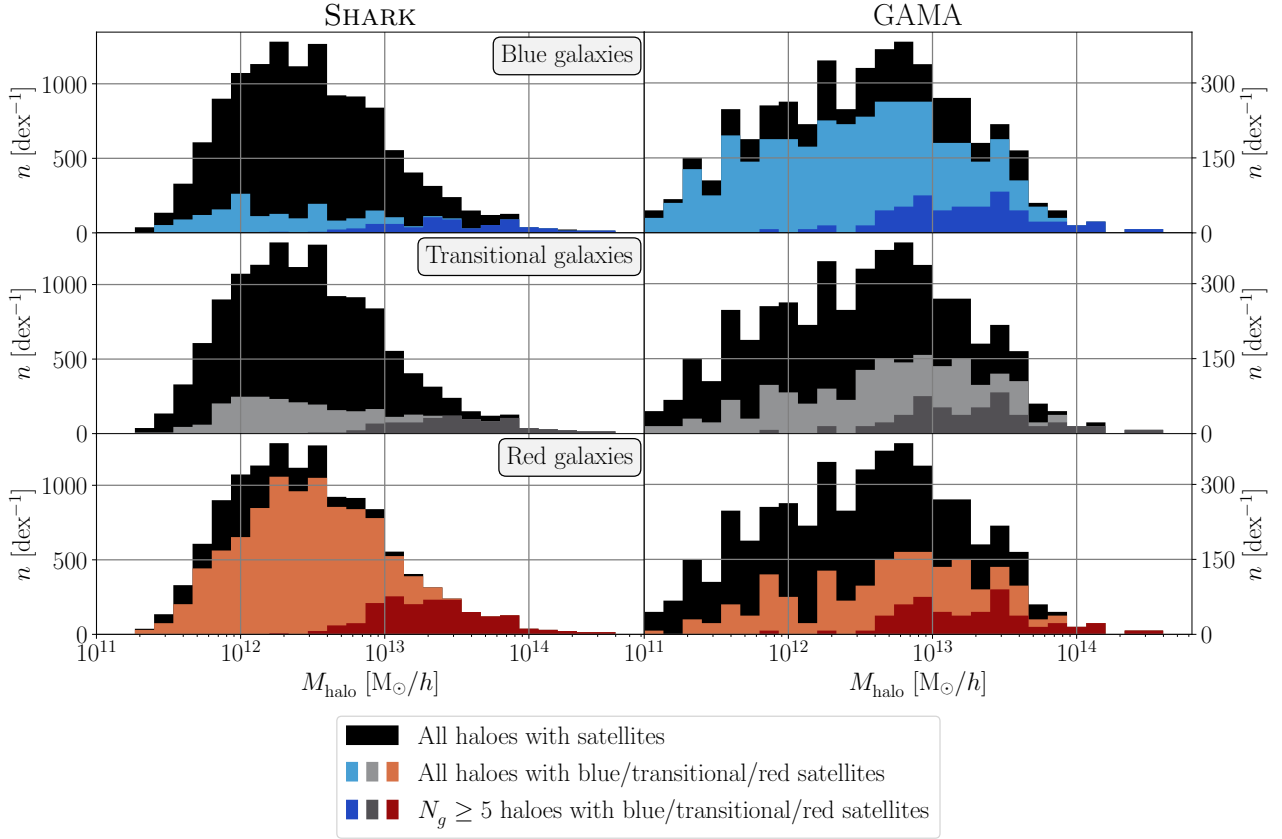


Figure 8. Comparison of the halo mass distribution from the GAMA and SHARK samples. SHARK is shown on the left column and GAMA on the right. In all panels, the black histograms indicate the distribution of all haloes hosting at least one satellite galaxy. The coloured histograms in the top/middle/bottom row show the mass distribution of haloes hosting at least one blue/transitional/red satellite. The lighter-coloured histograms show the distribution for all said haloes hosting at least one satellite, with the darker-coloured histograms the subset that hosts at least four satellites ($N_g \geq 5$). Note that both panels have different scales for the y-axis to focus on the effect of each selection rather than the different sizes of our samples.

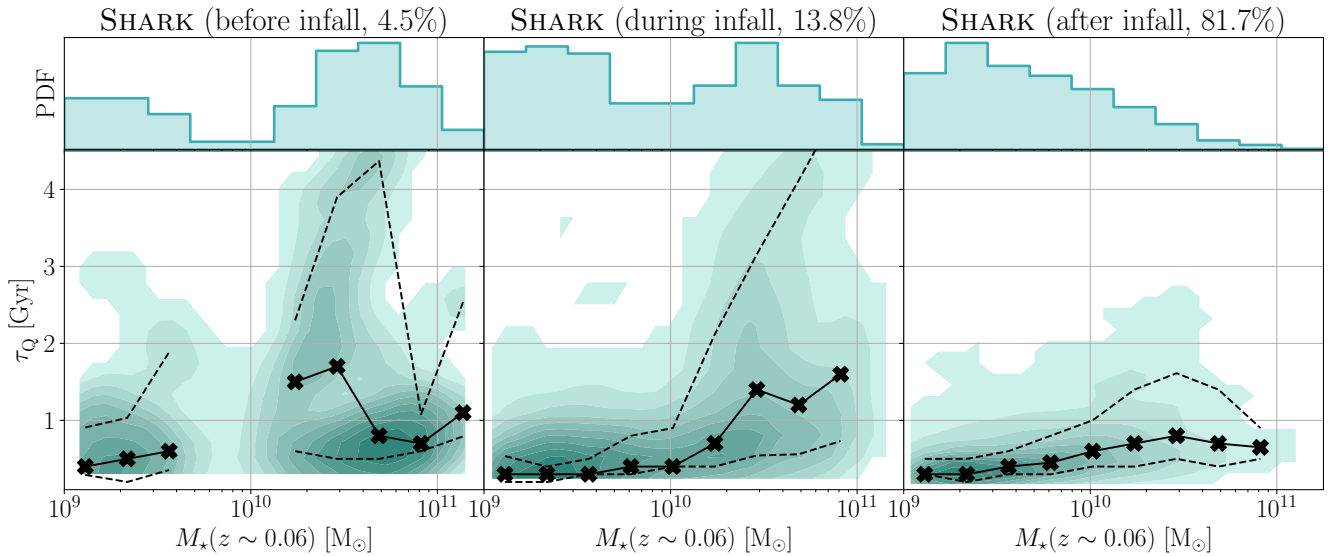


Figure 9. τ_Q of satellites in SHARK as a function of current stellar mass, and the stellar mass distribution, divided by when a galaxy became red relative to the time when the galaxy became a satellite. The percentage that each sample represents of the total of red satellites in SHARK is shown on the top labels of each column. Solid lines, dashed lines, markers and contours as in Figure 5.

(iii) were still blue when they became a satellite, i.e., transitioned in colour after infall, $t_{\text{LB, infall}} > t_{\text{LB, B}} > t_{\text{LB, R}}$.

The distribution of stellar mass and τ_{Q} for these categories are shown in Figure 9. It is clear that becoming a satellite is the main driver for galaxies to become red, as 81.7% of the red satellites in SHARK became red before after infall (iii). The stellar mass distribution of galaxies that became red before (i) and after infall show a marked difference, with those that became a satellite while in transition (ii) showing a distribution intermediate between the other two. SHARK galaxies that became red after infall have the shortest τ_{Q} , while those galaxies that became red before infall have the longest τ_{Q} . Galaxies that became a satellite while in transition show intermediate τ_{Q} relative to the other two groups.

5 DISCUSSION

5.1 Comparing our τ_{Q} definition with previous literature

Fundamental to any measurement of τ_{Q} is how it is defined. Measurements of τ_{Q} in the literature include derivation from star formation rates (e.g., Wetzel et al. 2013; Belli et al. 2019; Tacchella et al. 2022), galaxy colours (e.g., Schawinski et al. 2014; Trayford et al. 2016; Bremer et al. 2018; McNab et al. 2021), and spectral properties (e.g., Wheeler et al. 2014; Rowlands et al. 2018; Anghopo et al. 2019). Definitions include timescales to cross specific thresholds (e.g., Trayford et al. 2016; Bremer et al. 2018; Tacchella et al. 2022), e -folding timescales (e.g., Wetzel et al. 2013; Schawinski et al. 2014; Wheeler et al. 2014; Bremer et al. 2018), and inference from population densities or ages (e.g., Rowlands et al. 2018; Anghopo et al. 2020; McNab et al. 2021). Establishing how these different measurements compare is outside the scope of this work, so we only compare our τ_{Q} definition and measurements to those in the literature that are derived from galaxy colours. We remind the reader that differences in τ_{Q} definitions are not the only challenge in performing these comparisons. Modelling differences and shortcomings in the recovery of the true intrinsic galaxy colours can easily permeate both τ_{Q} definitions and measurements, so comparisons with literature results are also limited by underlying modelling differences.⁸

While definitions from observations abound (e.g., Schawinski et al. 2014; Smethurst et al. 2015; Bremer et al. 2018; Phillipps et al. 2019), differences in the recovery of the intrinsic stellar light result in significant differences in the loci of the colour populations. Table 3 provides a description of these selections, and the top row of Figure 10 shows how those from Schawinski et al. (2014) and Bremer et al. (2018); Phillipps et al. (2019) compare to ours. The issue of definitions that adopt a fixed parameterisation instead of being a function of population properties are clear here as the match to ours is strongly sample-driven. The Schawinski et al. (2014) green valley selection covers almost exclusively the red population for SHARK/SHARK_{fit}, and the Phillipps et al. (2019) covering mostly the

blue population for GAMA⁹. Furthermore, (to the author's knowledge) there are no observational selections that account for colour evolution with cosmic time, i.e., the selections are at fixed lookback time/redshift.

We now compare the classifications used for simulations by Trayford et al. (2016); Nelson et al. (2018); Wright et al. (2019) to the one we adopt for this work, shown in the bottom row of Figure 10. Trayford et al. (2016) classifies galaxies from the EAGLE simulation (Schaye et al. 2015) between red, green and blue using straight lines in the colour-mass plane, where only the normalisation evolves with time. While it does overlap most of the region we classify as transitional in GAMA, it is clearly slanted as a function of stellar mass compared to our statistically-based selection. The fixed nature of the selection limits also makes it a poor choice for SHARK/SHARK_{fit}, as it strongly overlaps the red population. The Trayford et al. (2016) selection limits are also consistently wider than our transitional region, save for SHARK above $\sim 10^{10.5} M_{\odot}$, which would lead to an over-estimation of τ_{Q} .

The classifications from Nelson et al. (2018) for IllustrisTNG and Wright et al. (2019) for EAGLE are more directly comparable to our classification, as they are all based on GMM fits to the colour population. Both define their green selection as:

$$G_{\text{upper}} = \mu_{\text{R}} - f\sigma_{\text{R}}, \quad (2)$$

$$G_{\text{lower}} = \mu_{\text{B}} + f\sigma_{\text{B}}, \quad (3)$$

where $\mu_{\{\text{B,R}\}}$ and $\sigma_{\{\text{B,R}\}}$ are the mean and standard deviation of the blue/red population, respectively, and f is a constant value. Nelson et al. (2018) adopts a value of $f = 1$, while Wright et al. (2019) adopts $f = 1.5$. For a fair comparison, we have used the $\mu_{\{\text{B,R}\}}$ and $\sigma_{\{\text{B,R}\}}$ we measured in Paper I to implement their selections, as the colour evolution in both EAGLE and IllustrisTNG may well not match those in GAMA and SHARK.

Both are in reasonable agreement with our classification for SHARK_{fit}, with Nelson et al. (2018) being a remarkable match, but the results for GAMA and SHARK show that this is just a lucky coincidence. In particular, in SHARK both criteria fail to reproduce our probabilistically-based classification, and at low masses they lead to an over-estimation of the transitional region. At high masses both criteria under-estimate τ_{Q} .

5.2 Comparing our τ_{Q} measurements between observations and simulations

A fundamental question to answer when exploring the τ_{Q} distribution is how it evolves with cosmic time. This can provide an insight into the physical processes behind the colour transformation of galaxies. A τ_{Q} distribution invariant with time would suggest that the different mechanisms and their relative prevalence are also time invariant. If τ_{Q} evolves with cosmic time instead, that suggests some combination of the following: different mechanisms operate at different times, the mechanisms' efficiency change with time, or that the relative mix of these mechanisms evolves with time.

As described in Section 4, the challenge in establishing whether τ_{Q} evolves with time is selection bias, irrespective of the chosen limits. Furthermore, galaxies of different current stellar masses could

⁸ It is worth noting that approaches based on relatively dust-insensitive spectral indexes (e.g., Rowlands et al. 2018; Anghopo et al. 2019) provide a different method to measure τ_{Q} . We do not include such studies in our comparisons as they are significantly different in at least one key aspect, like chosen space compared to our choice of $u - r - M_{\star}$ (e.g., Rowlands et al. 2018) or in the definition of the transitional region (e.g., Anghopo et al. 2019).

⁹ This is not to say that these are poor selections for the samples for which they were designed (see figures 4 and 1 of Schawinski et al. 2014; Phillipps et al. 2019, respectively), which we could only assess by implementing our method to their data sets.

Reference	Data type	Parameter space	Transition region lower limit	Transition region upper limit
Schawinski et al. (2014)	Observation	$(u-r)-M_{\star}$	$0.25 \log_{10}(M_{\star}/M_{\odot}) - 0.75$	$0.25 \log_{10}(M_{\star}/M_{\odot}) - 0.24$
Smethurst et al. (2015)	Observation	$(u-r)-r$	$-0.244 \tanh\left(\frac{r+20.07}{1.09}\right) + 20.6 - \sigma$	$-0.244 \tanh\left(\frac{r+20.07}{1.09}\right) + 20.6 + \sigma$
Trayford et al. (2016)	Simulation	$(u-r)-M_{\star}$	$0.2 \log_{10}(M_{\star}/M_{\odot}) - 0.25z^{0.6} - 0.3$	$0.2 \log_{10}(M_{\star}/M_{\odot}) - 0.25z^{0.6} + 0.24$
Bremer et al. (2018)	Observation	$(u-r)-M_{\star}$	$0.1 \log_{10}(M_{\star}/M_{\odot}) + 0.3$	$0.2 \log_{10}(M_{\star}/M_{\odot}) - 0.5$
Nelson et al. (2018)	Simulation	$(g-r)-M_{\star}$	$\mu_B + \sigma_B$	$\mu_R - \sigma_R$
Phillipps et al. (2019)	Observation	$(u-r)-M_{\star}$	$0.1 \log_{10}(M_{\star}/M_{\odot}) + 0.3$	$0.2 \log_{10}(M_{\star}/M_{\odot}) - 0.5$
Wright et al. (2019)	Simulation	$(u-r)-M_{\star}$	$\mu_B + 1.5\sigma_B$	$\mu_R - 1.5\sigma_R$
This work	Both	$(u-r)-M_{\star}$	$P_R > 0.02$	$P_R < 0.98$

Table 3. Sample of literature criteria to define the green valley/transition region. Our classification is at the end of the table for comparison purposes. Several remarks need to be made for a fair comparison. All literature definitions using observations include no time evolution and are valid only at low redshift ($z \leq 0.25$). The definition by [Smethurst et al. \(2015\)](#) references a dispersion (σ), but it is not clear what dispersion they used, besides that it seems to be independent of stellar mass (see their figure 3). [Bremer et al. \(2018\)](#) and [Phillipps et al. \(2019\)](#) use the same definition, but the former limits it to a narrow stellar mass range ($10^{10.25} < M_{\star}/M_{\odot} < 10^{10.75}$), while the latter expands it to their full sample. [Nelson et al. \(2018\)](#) and [Wright et al. \(2019\)](#) use the same type of criteria, but they chose difference factors for the standard deviation, whether this is a consequence of their different choices for colour or not is not clear. Note that $\mu_{\{B,R\}}$, $\sigma_{\{B,R\}}$, and P_R all are functions of lookback time, stellar mass and colour, see Section 3 for details.

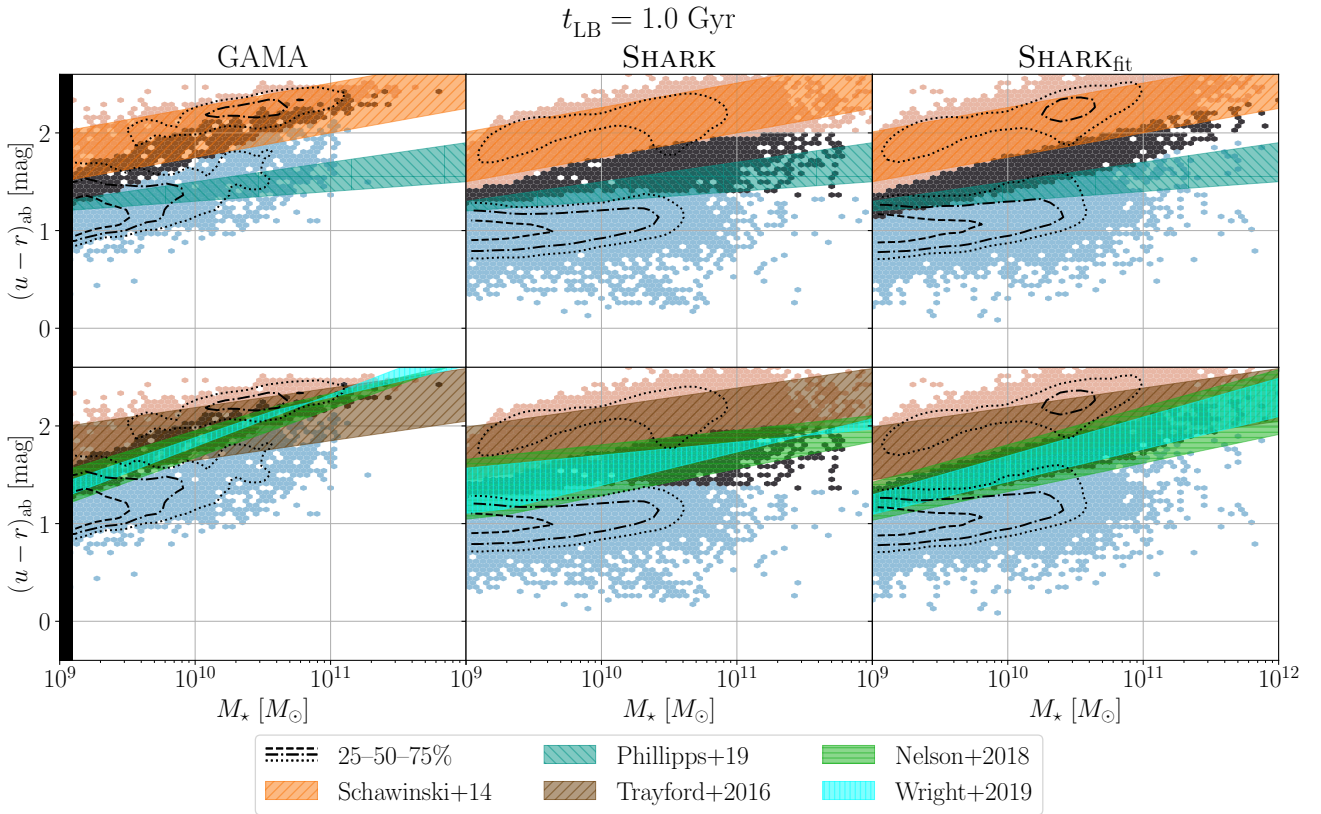


Figure 10. Comparison of the colour classification we adopt to two observational ([Schawinski et al. 2014](#); [Phillipps et al. 2019](#), top row; in orange and teal, respectively) and three theoretical ([Trayford et al. 2016](#); [Nelson et al. 2018](#); [Wright et al. 2019](#), bottom row; in brown, green, and cyan, respectively) literature examples. The comparison is made at the lowest lookback time of our data (1 Gyr), as a rough middle point between the redshift ranges of the literature classifications. Each column shows the classification for one of our samples, following the same thresholds as in Figure 2, with the underlying histogram bins being coloured in blue/grey/red if their median P_R of the galaxies classifies them as being blue/transitional/red. The dashed/dash-dotted/dotted contours indicate the highest density regions in each panel that contain 25/50/75% of the galaxies of each sample. The transitional region from the literature examples are shown by coloured bands in each panel. The black region in the left column indicates the stellar mass below the stellar mass completeness limit for GAMA (lies below $10^9 M_{\odot}$ for SHARK and SHARK_{fit}, further details in section 3.2 of [Paper I](#)). The classifications from [Nelson et al. \(2018\)](#) and [Wright et al. \(2019\)](#) are defined as functions of the means and standard deviations of each population, which is the reason why they are different across our samples.

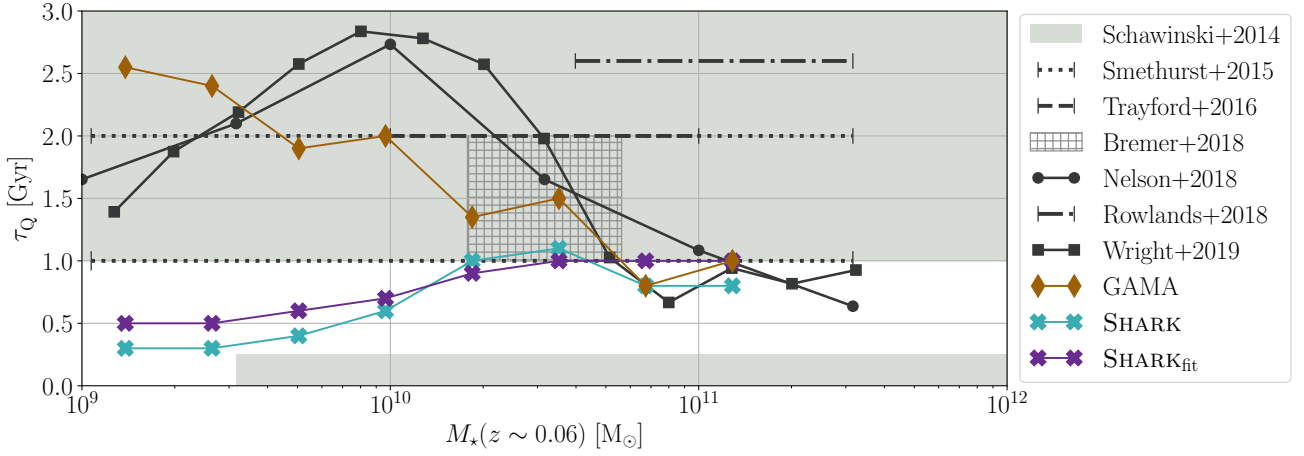


Figure 11. Comparison between the τ_Q we have measured in this work to a variety of literature results. Solid and hatched areas indicate results that only provide a range of values for τ_Q , together with the stellar mass range used in the work. Segmented lines indicate singular τ_Q values, with the extent of the line and markers on the edge the stellar mass range used to measure it. Solid lines indicate running medians of τ_Q as a function of stellar mass. Multiple lines may appear if the respective work provided more than one result. The results from this work are shown in colour, those from the literature in different shades of grey. Note that we show only one of the two measured τ_Q values from Rowlands et al. (2018), as the other lies outside our choice of range for τ_Q (~ 6.6 Gyr for $10^{11} < M_*/M_\odot < 10^{11.5}$)

have transitioned in colour at different lookback times. When accounting for both lookback time and stellar mass dependencies, we find that GAMA shows a clear evolution towards longer timescales at more recent cosmic times, while the same is not evident in SHARK. We do find a time evolution for τ_Q in SHARK_{fit}, unlike SHARK, which suggests that the difference between GAMA and SHARK may be attributable in to the process of SED fitting¹⁰. The difference in evolution of τ_Q as a function of stellar mass between GAMA and SHARK_{fit} suggests that some of this evolution might be real, instead of induced by our models in ProSPECT, though more work would be required to make a more conclusive statement.

Since the τ_Q distribution is broadly consistent for all three samples for $t_{LB,R} < 4$ Gyr, we can use that as a selection to study the connection between τ_Q and other galaxy properties. This selection means that we are roughly halving the number of galaxies that we can explore in SHARK/SHARK_{fit}, as galaxies above $\sim 10^{9.3} M_\odot$ exhibit a consistent median $t_{LB,R}$ of ~ 4 Gyr in these samples, but for GAMA we will only be able to explore a small fraction of $\sim 10^{10} M_\odot$ galaxies. Comparing the τ_Q - M_* distribution for all three samples, shown in Figure 11, shows that SHARK under-predicts τ_Q by up to ~ 2 Gyr for 10^9 - $10^{10.5} M_\odot$, with the tension being larger for lower stellar masses. Since the τ_Q distribution in SHARK_{fit} is in good agreement with that from SHARK, and that for masses above $\sim 10^{10.5} M_\odot$ all three samples show a good agreement, the difference between GAMA and SHARK at lower masses suggests that the mechanisms that quench these lower mass galaxies in SHARK are too efficient.

The red population in SHARK is strongly dominated by satel-

lites (71.4% of the sample), in apparent disagreement with GAMA (50.8%), but as shown in Paper I this is alleviated by accounting for observational confusion between centrals and satellites. Centrals and satellites below $\sim 10^{10.5} M_\odot$ in SHARK exhibit different τ_Q , but using a GAMA-like classification reduces the difference between both, suggesting that the similarity between centrals and satellites in GAMA could be due classification confusion. The choice of central/satellite classification cannot account for the strong difference in τ_Q between GAMA and SHARK/SHARK_{fit}, as satellites exhibit shorter transition timescales in SHARK/SHARK_{fit} than GAMA.

Since 83.2% of SHARK satellites became red after infall, this points to the quenching mechanisms for satellites in SHARK, the instantaneous stripping all halo gas of the galaxy, being too aggressive. A more gradual stripping of gas would allow satellites to replenish their interstellar medium (ISM) gas, increasing τ_Q (e.g., Font et al. 2008). Other SAMs have adopted gradual halo gas stripping models, usually combined with the inclusion of ISM stripping to balance the availability of gas for satellites (e.g., Font et al. 2008; Croton et al. 2006, 2016; Stevens & Brown 2017; Cora et al. 2018). More extreme models can also be found in the literature. E.g., in Henriques et al. (2015) satellites fully retain their halo gas and their ISM in haloes of masses lower than $10^{14} M_\odot$, leading to slow exhaustion of the gas to star formation. The latter was required by that model to reproduce the observed red fraction of galaxies. Based on these results, we will explore in future work if the combination of gradual halo gas stripping and ISM stripping leads to longer timescales than instantaneous halo gas stripping without ISM stripping.

SHARK satellites that became red before infall (i.e., that became red while being centrals) exhibit a similar τ_Q distribution as those of (current) central galaxies, but they show markedly different stellar mass distribution, with the former having a significant contribution from $\lesssim 10^{9.5} M_\odot$ galaxies. These low-mass satellites that became red as centrals exhibit starburst episodes prior to infall, indicating that the otherwise temporary gas exhaustion was made permanent by the instantaneous hot gas stripping in SHARK. Both low-mass

¹⁰ More detailed exploration is required to discern whether this evolution is a product of the SED fitting process, and if so, whether this evolution is a reflection of the more limited imprint that older stellar populations have on galaxy SEDs or a limitation of one or more of the models implemented in ProSPECT.

central and isolated red galaxies in GAMA exhibit long τ_Q relative to SHARK, suggesting that this is not the mechanism to reduce the tension between both. A possible improvement could be to extend the effectiveness of the AGN radio-mode feedback to lower halo masses in SHARK, as reducing the amount of gas available for cooling into the galaxy would lead to a gradual decrease of star formation (i.e., a long τ_Q).

5.3 Comparing our τ_Q measurements with literature results

What follows now is a series of comparisons with a representative collection of literature results, both from observations and simulations, which are also shown in Figure 11 as comparison to our results. Since the calculation of τ_Q could have a strong effect on the measured values, we include an overview of how they were derived. We remark that this means that good quantitative (or even qualitative) agreement should not be expected to be a natural result, as disagreements may well stem from methodological (or even conceptual) differences. Also, little discussion is presented on the possible lookback time dependence of τ_Q in the literature, so we will omit that aspect.

Starting with results from observations, Schawinski et al. (2014) inferred colour transition timescales combining colours and stellar masses of galaxies from the Sloan Digital Sky Survey (SDSS; York et al. 2000) with the morphological classification from Galaxy Zoo (Lintott et al. 2008). For this, they first divided their galaxy sample between "blue", "green" and "red" in the colour-stellar mass plane, with the limits being straight lines chosen by visual inspection (see Figure 10 and Table 3). They generated simple colour histories with an exponentially-decaying SFH with different e -folding timescales, and then compared the colour evolution from these SFHs to the colour-colour distribution of both early- and late-type galaxies. From these comparisons they inferred a fast transition for early-type galaxies ($\tau_Q \lesssim 250$ Myr), with late-type galaxies transitioning slowly ($\tau_Q \gtrsim 1$ Gyr). Since only $\sim 20\%$ of the GAMA sample shown in Figure 11 correspond to elliptical galaxies (according to the Driver et al. (2022) morphological classification), the expectation would be for our sample to better match the timescales that Schawinski et al. (2014) found for late-type galaxies, which is indeed the case. In contrast, SHARK/SHARK_{fit} show τ_Q in agreement with Schawinski et al. (2014) only for galaxies above $\sim 10^{10.5} M_\odot$, with galaxies below this mass exhibiting a median τ_Q neither consistent with early-type nor late-type galaxies. While Schawinski et al. (2014) find a dependence of τ_Q on halo mass for late-type galaxies, they do not find the same for the early-types that dominate the red population, which agrees with the similarity we find between low- and high-multiplicity groups in GAMA.

Smethurst et al. (2015) also used GALEX/SDSS photometry plus Galaxy Zoo morphological classification (though the more recent Galaxy Zoo2 release, Willett et al. 2013) to infer quenching timescales. They also classify galaxies as blue, green or red, but use instead the definition from Baldry et al. (2004), where everything $< 1\sigma$ from the local minimum in colour-magnitude as green. Furthermore, they also adopt a similar approach of generating sample colour evolution tracks from exponentially-decaying SFHs, though they use a Bayesian approach to find the timescale and quenching onset that best matches every galaxy in their sample. For bulge- and disc-dominated galaxies they find median timescales of ~ 1 and ~ 2 Gyr respectively, which is in good agreement with our results from GAMA. Their figures 8 and 11 suggest that these values

may be strongly driven by galaxies quenching early in the Universe ($t_{\text{LB,R}} > 6$ Gyr), which we do not explore in this work due to biases in the recovery. It is interesting to note that they seem to find a strong evolution toward longer timescales at more recent times (see their figures 8 through 11), though it is not clear if this is just a selection effect. Regardless, this qualitatively agrees with our findings in GAMA, where galaxies that become red more recently do it on longer timescales than those becoming red earlier.

Rowlands et al. (2018) used the strength of the 4000 Å break and the excess Balmer absorption from GAMA and the VIMOS Public Extragalactic Redshift Survey (VIPERS). They first divided galaxies as either post-starburst or not based on being above or below a Balmer absorption limit, and then further divided the non post-starburst between blue, green and red based on two ad hoc 4000 Å break values. They then measured the number density evolution of these classifications at a wide range of redshifts ($0.05 < z < 1.0$) to infer transition timescales at two partly overlapping stellar mass ranges ($> 10^{10.6} M_\odot$ and $> 10^{11} M_\odot$). They found transition timescale for green valley galaxies of $\sim 2.6/6.6$ Gyr for their mid/high-mass selection, independent of lookback time. This positive trend for timescales with stellar mass is opposite to our findings in GAMA, but it is likely driven by those being a different type of timescales, with the values themselves being significantly higher than seen in either GAMA or SHARK. This is likely because Rowlands et al. (2018) measure the timescale for $z \sim 0.7$ green valley galaxies would join the $z = 0$ red population, whereas we measure the timescale over which observed red galaxies became red, which Schawinski et al. (2014) shows are dominated by different morphological types.

Bremer et al. (2018) measured the fraction of galaxies in the green valley as a function of environment from GAMA, defined in colour-stellar mass space (see Figure 10 and Table 3), and combined it with the stellar ages of Taylor et al. (2011) to infer τ_Q^{11} . They limited their analysis to galaxies with stellar masses in the $10^{10.25} - 10^{10.75} M_\odot$ range, $0.1 < z < 0.2$ and r -band axial ratio $b/a > 0.5$. They found a τ_Q of $\sim 1-2$ Gyr, in good agreement with our measurement of τ_Q for GAMA. Also similar to our results from GAMA, they found no evidence for environmental effect from the near-constant fraction of green valley galaxies as a function of group multiplicity¹², but our results from SHARK show that central/satellite confusion can strongly diminish any environmental signature present in τ_Q .

We now focus on a comparison with literature results presented for galaxy formation simulations. Trayford et al. (2016) used galaxies with stellar masses of $10^{10} - 10^{11} M_\odot$ from the EAGLE simulation (Schaye et al. 2015), and classifying them as blue, green or red by ad hoc colour selections, defined as a function of both stellar mass and redshift (see Figure 10 and Table 3). From these, they selected $z = 0$ red galaxies and measured the timescale over which they transition from blue to red. They found a median τ_Q of ~ 2 Gyr, though with a distribution strongly skewed towards shorter

¹¹ A similar method was also presented in Phillipps et al. (2019), but instead they used the e -folding time from the Taylor et al. (2011) fits to infer how long will current green galaxies take to become red. This is the reason why we do not discuss their results, to avoid comparisons between our *reconstructed* evolution to their *predicted* evolution.

¹² They do find evidence that galaxies in high density environment have shorter lifespans as part of the blue population than in less dense environment, suggesting that a richer environment will trigger an earlier transition to red.

timescales, with a peak closer to ~ 1.5 Gyr. While they do not find a strong difference in the median τ_Q for centrals and satellites (order of a few hundred Myr), the distributions shown in their figure 10 indicate that centrals are less skewed to short timescales. SHARK does display the same trend, though we find shorter τ_Q (factor of ~ 3). Their results are in agreement with our results from GAMA, but it is not clear if this holds for earlier times, as they do not explore the time evolution of τ_Q . They do not find evidence of a strong dependence with stellar mass, which seems in better agreement with SHARK than GAMA. Finally, we find in SHARK the same results that they do with regards to satellites: the majority become red when becoming a satellite.

Nelson et al. (2018) employed a similar method to ours to measure τ_Q from the IllustrisTNG simulation (Pillepich et al. 2018), first characterising the colour population with two Gaussian components, with parameters as function of stellar mass and redshift. They then defined the limits for each population, set at 1σ from the mean of each population, which is the most significant difference with our probability-based approach (see Figure 10 and Table 3). Like Trayford et al. (2016), they also found an asymmetrical τ_Q distribution, skewed to shorter values, finding similar median and peak values (~ 2 and ~ 1.6 Gyr, respectively). They found a dependence with stellar mass, with τ_Q peaking for galaxies of $\sim 10^{10} M_\odot$. While the range of median τ_Q values they measure coincides with that from GAMA, we find a different trend with stellar mass, with the best agreement being for galaxies $\geq 10^{10.5} M_\odot$. They also found a weak trend for centrals below $10^{10} M_\odot$ to take longer to become red than satellites.

Also using galaxies from the EAGLE simulation, Wright et al. (2019) used a classification close to that used by Nelson et al. (2018), finding τ_Q to be in the ~ 2 – 4 Gyr range, depending on both stellar mass and environment. They found different τ_Q for centrals and satellites for galaxies below $\sim 10^{10.5} M_\odot$ (~ 4 and ~ 2 Gyr respectively), with timescales showing an inverted U-shape and both centrals and satellites peaking at $\sim 10^{9.7} M_\odot$. For larger stellar masses they found all galaxies to have similar τ_Q (~ 2 Gyr). Their τ_Q measurements are in strong agreement with those of Nelson et al. (2018), despite using different thresholds to measure τ_Q (see Table 3), which suggests that the stellar mass trend of τ_Q found in both works may be a consequence of how they define the limits of the blue and red populations.

6 CONCLUSIONS

In this work, we have used the characterisation of the colour evolution of the blue and red galaxy populations we presented in Paper I, to calculate upper limits for τ_Q on which red galaxies transitioned from being blue to red. For this, we first calculated the probability of all galaxies in our three samples (GAMA, SHARK and SHARK_{fit}) to belong to the red population, then used the distribution of this probability to define the values between which we will measure τ_Q . Accounting for selection biases, we find evidence that τ_Q evolves with time only in GAMA, with τ_Q increasing from ~ 1 to ~ 3 Gyr in a time span of ~ 4 Gyr (in SHARK/SHARK_{fit} τ_Q remains stable at ≤ 1 Gyr). Our observations and simulations do not agree on whether there is a stellar mass dependence on the lookback time when they became red, with the former in agreement with a large body of existing literature that current high-mass galaxies became red before low-mass galaxies (i.e., downsizing), while the latter fails

to reproduce such trend. We find a difference between centrals and satellites in GAMA only for $M_\star \lesssim 10^{10} M_\odot$, with satellites showing $\tau_Q \sim 0.4$ Gyr shorter than centrals. The results from SHARK suggest the possibility of a larger difference being hidden by observational central/satellite classification confusion. Finally, we find that assuming an instantaneous halo gas stripping in SHARK is the likely driver for the shorter-than-observed τ_Q for satellites.

ACKNOWLEDGEMENTS

We thank Chris Power and Pascal Elahi for their role in completing the SURFS *N*-body DM-only simulations suite, Rodrigo Tobar for his contributions to SHARK, Andrea Cattaneo and Benjamin Johnson for the comments and feedback provided to the doctoral thesis on which this work is based, Ruby Wright for providing the data from Wright et al. (2019) for Figure 11.

MB acknowledges the support of the University of Western Australia through a Scholarship for International Research Fees and Ad Hoc Postgraduate Scholarship, and the funding by McMaster University through the William and Caroline Herschel Fellowship. LJMD and ASGR acknowledge support from the Australian Research Councils Future Fellowship scheme (FT200100055 and FT200100375, respectively). CdPL is funded by the ARC Centre of Excellence for All Sky Astrophysics in 3 Dimensions (ASTRO 3D), through project number CE170100013. CdPL also thanks the MERAC Foundation for a Postdoctoral Research Award. SB acknowledges support by the Australian Research Council's funding scheme DP180103740. JET is supported by the Australian Government Research Training Program (RTP) Scholarship.

This work was supported by resources provided by the Pawsey Supercomputing Centre with funding from the Australian Government and the Government of Western Australia. We gratefully acknowledge DUG Technology for their support and HPC services.

GAMA is a joint European-Australasian project based around a spectroscopic campaign using the Anglo-Australian Telescope. The GAMA input catalogue is based on data taken from the Sloan Digital Sky Survey and the UKIRT Infrared Deep Sky Survey. Complementary imaging of the GAMA regions is being obtained by a number of independent survey programmes including GALEX MIS, VST KiDS, VISTA VIKING, WISE, Herschel-ATLAS, GMRT and ASKAP providing UV to radio coverage. GAMA is funded by the STFC (UK), the ARC (Australia), the AAO, and the participating institutions. The GAMA website is <http://www.gama-survey.org/>. Based on observations made with ESO Telescopes at the La Silla Paranal Observatory under programme ID 179.A-2004. Based on observations made with ESO Telescopes at the La Silla Paranal Observatory under programme ID 177.A-3016.

The analysis on this work was performed using the programming languages PYTHON v3.10 (<https://www.python.org>), with the open source packages MATPLOTLIB v3.7 (Hunter 2007), NUMPY v1.24 (Harris et al. 2020), PANDAS v1.5 (pandas development team 2022), SCICM v1.0 (<https://github.com/MBravoS/scicm>), SciPY v1.10 (Virtanen et al. 2020), and SLOTC v0.6 (<https://github.com/MBravoS/splotch>), in addition of the software previously described.

DATA AVAILABILITY

The P_R tracks and τ_Q catalogues generated for this work will be shared on reasonable request to the corresponding author. For all other data, see the Data Availability statement in [Paper I](#).

REFERENCES

- Anghopo J., Ferreras I., Silk J., 2019, *MNRAS*, **488**, L99
- Anghopo J., Ferreras I., Silk J., 2020, *MNRAS*, **495**, 2720
- Baldry I. K., Glazebrook K., Brinkmann J., Ivezić Ž., Lupton R. H., Nichol R. C., Szalay A. S., 2004, *ApJ*, **600**, 681
- Baldry I. K., Balogh M. L., Bower R. G., Glazebrook K., Nichol R. C., Bamford S. P., Budavari T., 2006, *MNRAS*, **373**, 469
- Bell E. F., et al., 2004, *ApJ*, **608**, 752
- Belli S., Newman A. B., Ellis R. S., 2019, *ApJ*, **874**, 17
- Bellstedt S., et al., 2020, *MNRAS*, **498**, 5581
- Bellstedt S., et al., 2021, *MNRAS*, **503**, 3309
- Bershady M. A., Jangren A., Conselice C. J., 2000, *AJ*, **119**, 2645
- Blanton M. R., 2006, *ApJ*, **648**, 268
- Blanton M. R., et al., 2003, *ApJ*, **594**, 186
- Boquien M., Burgarella D., Roehly Y., Buat V., Ciesla L., Corre D., Inoue A. K., Salas H., 2019, *A&A*, **622**, A103
- Bower R. G., Benson A. J., Malbon R., Helly J. C., Frenk C. S., Baugh C. M., Cole S., Lacey C. G., 2006, *MNRAS*, **370**, 645
- Bravo M., Lagos C. d. P., Robotham A. S. G., Bellstedt S., Obreschkow D., 2020, *MNRAS*, **497**, 3026
- Bravo M., Robotham A. S. G., Lagos C. d. P., Davies L. J. M., Bellstedt S., Thorne J. E., 2022, *MNRAS*, **511**, 5405
- Bremer M. N., et al., 2018, *MNRAS*, **476**, 12
- Brinchmann J., Ellis R. S., 2000, *ApJ*, **536**, L77
- Bruzual G., Charlot S., 2003, *MNRAS*, **344**, 1000
- Carnall A. C., McLure R. J., Dunlop J. S., Davé R., 2018, *MNRAS*, **480**, 4379
- Cattaneo A., Dekel A., Devriendt J., Guiderdoni B., Blaizot J., 2006, *MNRAS*, **370**, 1651
- Chauhan G., Lagos C. d. P., Stevens A. R. H., Bravo M., Rhee J., Power C., Obreschkow D., Meyer M., 2021, arXiv e-prints, p. [arXiv:2102.12203](https://arxiv.org/abs/2102.12203)
- Coil A. L., et al., 2008, *ApJ*, **672**, 153
- Cora S. A., et al., 2018, *MNRAS*, **479**, 2
- Cowie L. L., Songaila A., Hu E. M., Cohen J. G., 1996, *AJ*, **112**, 839
- Croton D. J., et al., 2006, *MNRAS*, **365**, 11
- Croton D. J., et al., 2016, *The Astrophysical Journal Supplement Series*, **222**, 22
- Driver S. P., et al., 2006, *MNRAS*, **368**, 414
- Driver S. P., et al., 2011, *MNRAS*, **413**, 971
- Driver S. P., et al., 2022, *MNRAS*, **513**, 439
- Faber S. M., et al., 2007, *ApJ*, **665**, 265
- Font A. S., et al., 2008, *MNRAS*, **389**, 1619
- Harris C. R., et al., 2020, *Nature*, **585**, 357
- Heavens A., Panter B., Jimenez R., Dunlop J., 2004, *Nature*, **428**, 625
- Henriques B. M. B., White S. D. M., Thomas P. A., Angulo R., Guo Q., Lemson G., Springel V., Overzier R., 2015, *MNRAS*, **451**, 2663
- Hunter J. D., 2007, *Computing In Science & Engineering*, **9**, 90
- Johnson B. D., Leja J., Conroy C., Speagle J. S., 2021, *ApJS*, **254**, 22
- Kauffmann G., White S. D. M., Heckman T. M., Ménéard B., Brinchmann J., Charlot S., Tremonti C., Brinkmann J., 2004, *MNRAS*, **353**, 713
- Kaviraj S., Schawinski K., Silk J., Shabala S. S., 2011, *MNRAS*, **415**, 3798
- Lagos C. D. P., Cora S. A., Padilla N. D., 2008, *MNRAS*, **388**, 587
- Lagos C. d. P., Tobar R. J., Robotham A. S. G., Obreschkow D., Mitchell P. D., Power C., Elahi P. J., 2018, *MNRAS*, **481**, 3573
- Lagos C. d. P., et al., 2019, *MNRAS*, **489**, 4196
- Lintott C. J., et al., 2008, *MNRAS*, **389**, 1179
- Liske J., et al., 2015, *MNRAS*, **452**, 2087
- Martin D. C., et al., 2007, *ApJS*, **173**, 342
- McNab K., et al., 2021, *MNRAS*, **508**, 157
- Mignoli M., et al., 2009, *A&A*, **493**, 39
- Nelson D., et al., 2018, *MNRAS*, **475**, 624
- Noll S., Burgarella D., Giovannoli E., Buat V., Marcellac D., Muñoz-Mateos J. C., 2009, *A&A*, **507**, 1793
- Pasquali A., Smith R., Gallazzi A., De Lucia G., Zibetti S., Hirschmann M., Yi S. K., 2019, *MNRAS*, **484**, 1702
- Peng Y.-j., et al., 2010, *ApJ*, **721**, 193
- Phillipps S., et al., 2019, *MNRAS*, **485**, 5559
- Pillepich A., et al., 2018, *MNRAS*, **473**, 4077
- Planck Collaboration et al., 2016, *A&A*, **594**, A13
- Robotham A. S. G., et al., 2011, *MNRAS*, **416**, 2640
- Robotham A. S. G., Bellstedt S., Lagos C. d. P., Thorne J. E., Davies L. J., Driver S. P., Bravo M., 2020, *MNRAS*, **495**, 905
- Rowlands K., et al., 2018, *MNRAS*, **473**, 1168
- Schawinski K., et al., 2014, *MNRAS*, **440**, 889
- Schaye J., et al., 2015, *MNRAS*, **446**, 521
- Smethurst R. J., et al., 2015, *MNRAS*, **450**, 435
- Stevens A. R. H., Brown T., 2017, *MNRAS*, **471**, 447
- Strateva I., et al., 2001, *AJ*, **122**, 1861
- Tacchella S., et al., 2022, *ApJ*, **926**, 134
- Taylor E. N., et al., 2011, *MNRAS*, **418**, 1587
- Taylor E. N., et al., 2015, *MNRAS*, **446**, 2144
- Thorne J. E., et al., 2021, *MNRAS*, **505**, 540
- Thorne J. E., et al., 2022, *MNRAS*, **509**, 4940
- Trayford J. W., et al., 2015, *MNRAS*, **452**, 2879
- Trayford J. W., Theuns T., Bower R. G., Crain R. A., Lagos C. d. P., Schaller M., Schaye J., 2016, *MNRAS*, **460**, 3925
- Virtanen P., et al., 2020, *Nature Methods*, **17**, 261
- Weinmann S. M., van den Bosch F. C., Yang X., Mo H. J., Croton D. J., Moore B., 2006, *MNRAS*, **372**, 1161
- Wetzel A. R., Tinker J. L., Conroy C., van den Bosch F. C., 2013, *MNRAS*, **432**, 336
- Wheeler C., Phillips J. I., Cooper M. C., Boylan-Kolchin M., Bullock J. S., 2014, *MNRAS*, **442**, 1396
- Willett K. W., et al., 2013, *MNRAS*, **435**, 2835
- Williams R. J., Quadri R. F., Franx M., van Dokkum P., Labbé I., 2009, *ApJ*, **691**, 1879
- Wolf C., Meisenheimer K., Rix H. W., Borch A., Dye S., Kleinheinrich M., 2003, *A&A*, **401**, 73
- Wright R. J., Lagos C. d. P., Davies L. J. M., Power C., Trayford J. W., Wong O. I., 2019, *MNRAS*, **487**, 3740
- Wyder T. K., et al., 2007, *ApJS*, **173**, 293
- York D. G., et al., 2000, *AJ*, **120**, 1579
- da Cunha E., Charlot S., Elbaz D., 2008, *MNRAS*, **388**, 1595
- pandas development team T., 2022, pandas-dev/pandas: Pandas, doi:10.5281/zenodo.7093122, <https://doi.org/10.5281/zenodo.7093122>

APPENDIX A: RECOVERY OF τ_Q FROM SHARK WITH PROSPECT

Figure A1 shows the recovery of $t_{LB,B}$, $t_{LB,R}$, and τ_Q of SHARK galaxies using PROSPECT. In general, we find small median biases in the recovery of τ_Q ($\lesssim 0.03$ Gyr) but we find a large scatter in the recovery (16th–84th percentile range of ~ 1.1 Gyr), indicating that the population as a whole is reasonably recovered but not individual galaxies. τ_Q is better recovered than either $t_{LB,B}$ or $t_{LB,R}$, e.g., we better recover *how fast* galaxies become red rather than *when* they leave (enter) the blue (red) population.

We find that $\Delta\tau_Q$ trends with other properties, like stellar mass or infall category (see Section 4.3), are almost completely accounted for by the central/satellite classification, with centrals showing a worse recovery than satellites. E.g., we find that τ_Q recovery worsens with increasing mass, and that category (iii) satellites are better recovered than those in category (i), but those are a consequence

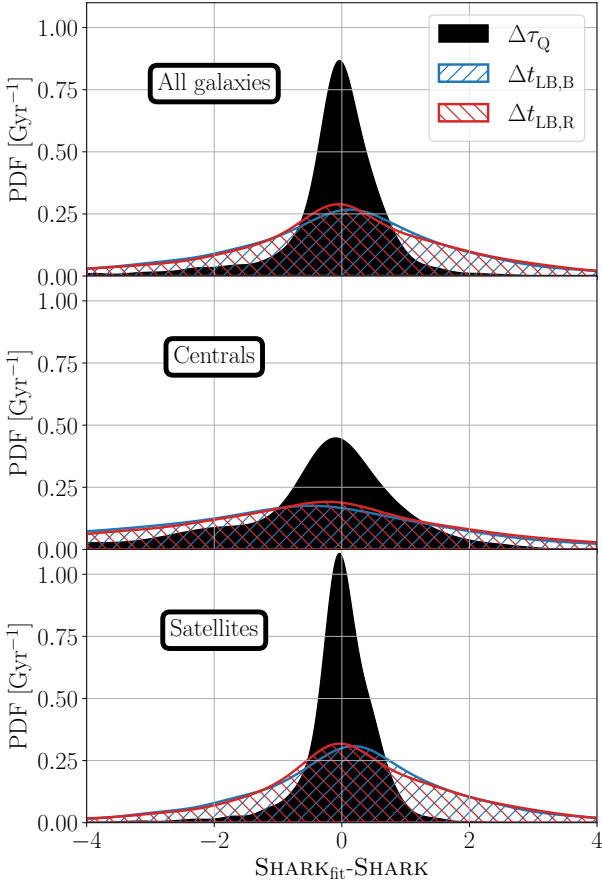


Figure A1. Recovery of $t_{\text{LB,B}}$ (in hatched blue), $t_{\text{LB,R}}$ (hatched red), and τ_{Q} (solid black) from SHARK red galaxies with PROSPECT. To avoid visualisation artefacts due to the discreteness of all three values shown ($\Delta t_{\text{LB,B}}$, $\Delta t_{\text{LB,R}}$, and $\Delta \tau_{\text{Q}}$), the PDFs shown have been constructed using the `gaussian_kde` Gaussian Kernel Density Estimator (KDE) function from `scipy`. **Matías: maybe add a few statistics to each panel?**

of the dominating type of galaxies as a function of stellar mass and that category (iii)/(i) galaxies quenched as satellites/centrals. The one exception to this are $\sim 10^{10.5} M_{\odot}$ centrals, which are the main driver for the skew towards under-estimated τ_{Q} values. The difference between centrals and satellites is likely a consequence of the SFH model we use in PROSPECT, a skewed-Gaussian SFH, being better suited to model the quenching of the latter. This should not be necessarily understood as rejuvenation being a key factor, as few red galaxies undergo a rejuvenation episode ($\lesssim 3\%$, see appendix A of Paper I), but rather that limited gas replenishment can extend the time quenching in a manner that is not well-captured by a skewed Gaussian.

We also tested a different choice for $t_{\text{LB,B}}$ than the one outlined in Section 4, using the first time the galaxy left the blue population instead of the last. This was motivated by the assumption that the skewed Normal SFH we adopt in PROSPECT would more likely recover a smooth proxy of the true SHARK SFHs, with the longer τ_{Q} definition leading to a better match with SHARK_{fit}. We found the opposite to be true, with this longer τ_{Q} definition leading to a strong bias in the recovery of both $t_{\text{LB,B}}$ and τ_{Q} ($\sim 1\text{--}2$ Gyr, depending on stellar mass), with the shorter definition leading to a less biased

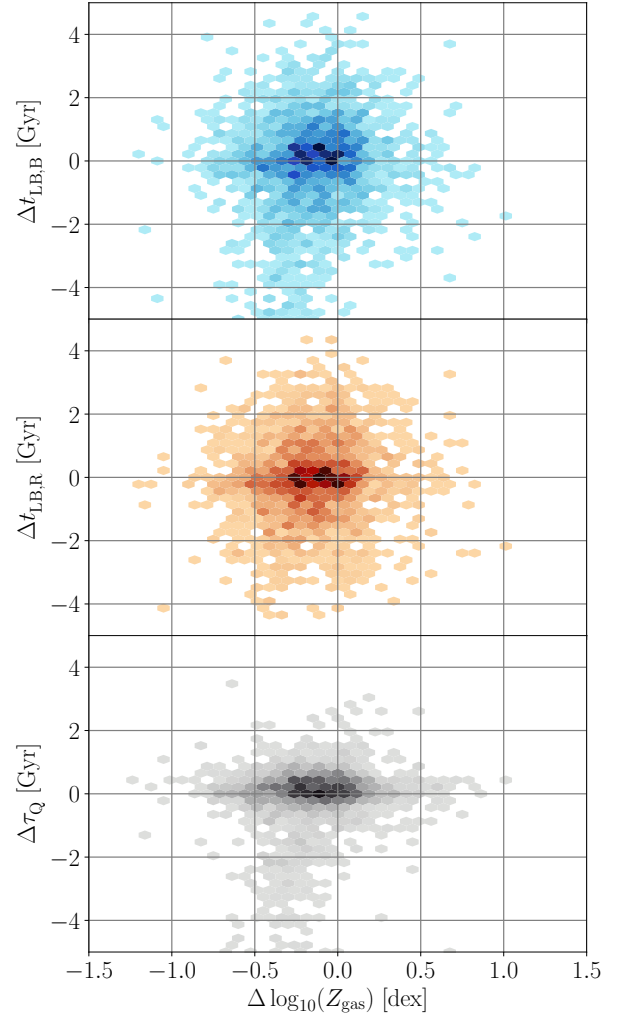


Figure A2. Relation between the recovery of the gas-phase metallicity, Z_{gas} , to the recovery of $t_{\text{LB,B}}$ (top panel), $t_{\text{LB,R}}$ (middle), and τ_{Q} (bottom) with PROSPECT. The colour of the bins indicate the number of galaxies with a linear scaling. For $\Delta t_{\text{LB,B}}$ and $\Delta \tau_{\text{Q}}$ a few ($\lesssim 1.5\%$) lie below their respective y-axis lower limits.

recovery (see Appendix A). This finding suggests that our choice of SFH is robust against multiple episodes of significant star formation and provides a sensible recovery of the last quenching episode¹³, which we have verified by examining individual SED fits against the true evolution in SHARK.

SHARK galaxies that remain for an extended period in the transitional region have proven to be a more significant challenge, as can be seen in Figures 4 and 6. The bottom panel in Figure A2 shows that, while there is no particular correlation between $\Delta \tau_{\text{Q}}$ and the gas-phase metallicity (Z_{gas}) for most galaxies, galaxies with $\Delta \tau_{\text{Q}} \lesssim -2$ Gyr show a systematic bias in the recovery of Z_{gas} . From the upper and middle panels in Figure A2 clearly indicate that the error in τ_{Q}

¹³ Which is not to say that the overall evolution of the galaxy would be well-recovered, which depends on how well the overall evolution of the galaxy can be approximated with the models adopted in PROSPECT.

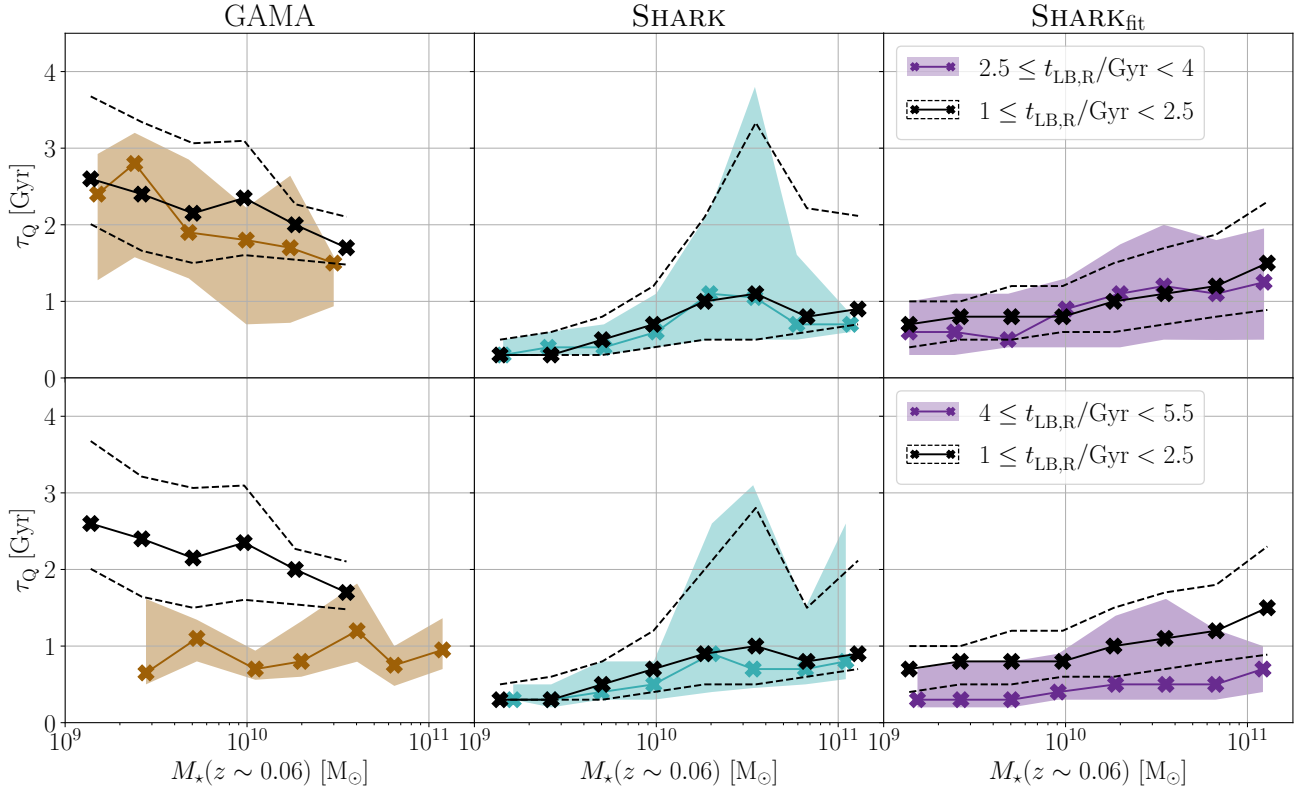


Figure A3. Comparison between the τ_Q measured at two different lookback time bins with a comparable $t_{\text{LB,R}}-\tau_Q$ selection. The top row compares the τ_Q distribution between the $1 \leq t_{\text{LB,R}}/\text{Gyr} < 2.5$ and $2.5 \leq t_{\text{LB,R}}/\text{Gyr} < 4$ bins, the bottom row between $1 \leq t_{\text{LB,R}}/\text{Gyr} < 2.5$ and $4 \leq t_{\text{LB,R}}/\text{Gyr} < 5.5$. The solid lines indicate the τ_Q running median, and the dashed lines and shaded areas the 16-84th percentiles, with those in colour being measured at the respective $t_{\text{LB,R}}$ bins and those in black from the lowest $t_{\text{LB,R}}$ bin. Each column shows the results for a different sample, left to right: GAMA, SHARK, and SHARK_{fit}.

is driven by errors in $t_{\text{LB,B}}$, indicating that these galaxies are being recovered as star-forming for a longer period than in SHARK.

This finding is in line with the difference between the true and recovered SFHs shown in figure A.1 in Paper I. These are $\geq 10^{10.5} M_\odot$, $\tau_Q \geq 2$ Gyr galaxies (see Figure 6), which correspond to the galaxies we highlighted in appendix A.3 of Paper I as particularly challenging to fit. We found that this stems from dust properties of these bulge-dominated galaxies, with steep dust attenuation slopes (relative to discs) that proved challenging to recover with our current modelling choices in PROSPECT, leading to biases also in their recovered SFHs and ZHs. This is unlikely to significantly affect our measurements and conclusions, since the SHARK_{fit} results indicate that this only leads to an underestimation in the dispersion of τ_Q .

APPENDIX B: CORROBORATION OF THE TIME EVOLUTION OF τ_Q , OR LACK OF THEREOF

To explore if any of our samples display a time-dependent τ_Q distribution, when comparing two lookback time bins set a limit to the maximum τ_Q included in the comparison. This is to remove the possible bias due to the larger span of τ_Q values that we can measure at the lower lookback time bin. I.e., when comparing the $1 \leq t_{\text{LB,R}}/\text{Gyr} < 2.5$ and $2.5 \leq t_{\text{LB,R}}/\text{Gyr} < 4$ bins, we set the upper τ_Q limit for both bins at 6 Gyr, as that is the largest τ_Q we can

measure at a lookback time of 4 Gyr given our chosen starting point of 10 Gyr (Section 2). This process ensures an equal τ_Q completeness for the two lookback time bins being compared, enabling us to study whether the τ_Q distribution evolves with cosmic time or not.

Figure A3 shows the measured τ_Q as a function of stellar mass at two different $t_{\text{LB,R}}$ bins ($2.5 \leq t_{\text{LB,R}}/\text{Gyr} < 4$ and $4 \leq t_{\text{LB,R}}/\text{Gyr} < 5.5$) and compares them to the lowest $t_{\text{LB,R}}$ bin ($1 \leq t_{\text{LB,R}}/\text{Gyr} < 2.5$). SHARK shows a strong consistency when comparing similarly-selected samples at different lookback times, indicating that τ_Q does not depend on lookback time for this sample. In contrast, GAMA exhibits a strong evolution. Galaxies with $M_\star < \sim 10^{10.5} M_\odot$ that became red at a lookback time of 4–5.5 Gyr have τ_Q values that are a factor of ~ 2 shorter than those of similarly-selected galaxies that transitioned in the 1–2.5 Gyr range, with galaxies above that stellar mass showing a smaller evolution in τ_Q . A similar decrease by a factor of ~ 2 is evident in SHARK_{fit}, though without the stellar mass dependence seen in GAMA. While this suggests that this evolution is at least partially due to our modelling choices in PROSPECT, it is not obvious that this can fully explain it, as GAMA and SHARK_{fit} display different mass dependencies and measured timescales.

This paper has been typeset from a \LaTeX file prepared by the author.